11

Multiscale models of the vascular system

Luca Formaggia, Alfio Quarteroni, and Alessandro Veneziani

As we have illustrated in the previous chapters, there are essentially three classes of models for the vascular system: fully three dimensional models, based on the Navier-Stokes (NS) equations, one dimensional models, including the space dependence on the vessel axial coordinate, based on the Euler (E) equations, and the lumped parameter or zero-dimensional models, based on the Kirchhoff laws (K) for hydraulic networks. Navier-Stokes based models can account for many different features of blood flow problems, such as the blood rheology (Chapter 6), the vascular wall dynamics (Chapter 3), the interaction between blood flow and wall deformation (Chapters 8 and 9). These models are perfectly adequate for investigating qualitatively and quantitatively the effects of the geometry on the blood flow (Chapters 5) and the possible relations between local haemodynamics and the development of some pathologies (Chapter 1). On the other hand, the high computational costs (Chapters 2, 3 and 9) restrict their use to cover few contiguous vascular districts only.

Euler-based models provide an optimal tool for the analysis of wave propagation phenomena in the vascular tree. In particular, they are convenient when the local flow details are less relevant than the accounting for propagative phenomena on large parts of the vascular tree and the numerical results are needed in a relatively short time. These models outline the role of the vascular system as a sort of telegraph line with the task of transmitting nutrients as well as biological signals along the body. On the other hand, the space dependence still retained in these models inhibits their use in the whole vascular system. In fact, it would be impossible to follow the geometrical details of the capillary network (not to mention the specific rheological assumptions required by capillary circulation – see Chapter 6).

On the contrary, Kirchhoff-based models can provide a representation of a large part or even the whole circulatory system, since they get rid of the explicit space dependence (see Section 10.2 and [364]). In a simple and however still quantitative way, these models can include the presence of the heart, the venous system, but also account for self-regulating and metabolic dynamics, as we have seen in Section 10.2.4.

Formaggia L, Quarteroni A, Veneziani A (Eds.): Cardiovascular Mathematics. Modeling and simulation of the circulatory system

If NS, E and K models provide such a different tools, reliable numerical methods for real life applications need to overcome the drawbacks and weakness of each individual class of models. This can be done by resorting to the *geometrical multiscale representation* of the circulatory system.

11.1 What do we mean with *geometrical multiscale models*?

Geometrical multiscale[1] approach is a strategy for modelling the circulatory system, including the reciprocal interactions between local and systemic haemodynamics by exploiting the complementary features of the different possible models. Indeed, these features suggest in a natural way to couple detailed local models with coarser models able to describe the dynamics over a large part or the whole system with acceptable computational costs (see Fig. 11.1).

Multiscale modelling can be regarded as a refinement of models, or a sort of "models zoom" in a specific region of interest, moving from a rough description of the whole system (*bottom-up approach*). From a different point of view, it

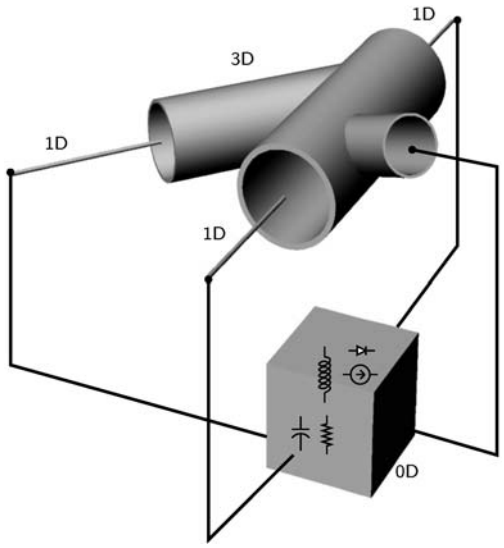

Fig. 11.1. A schematic representation of a geometrical multiscale model

[1] Term "multiscale" is often used with a different meaning in many fields of mathematical and numerical modelling, whenever two or more time and/or spatial scales are present. Typical examples are the modelling of turbulence or multiresolution representations. In order to avoid ambiguities, we have added the term *geometrical* for identifying the multiscale perspective illustrated in this chapter.

can be regarded as a sophisticated and reliable method for computing correct boundary conditions at the artificial boundaries of a district of interest, that is the non-physical boundaries needed to bound the computational domain (*top-down approach*). In the latter perspective, it can be considered also as a specific numerical tool to avoiding, or at least reduce, spurious effects caused by the presence of artificial boundaries (see also Chapter 2). Indeed, the propagative nature of blood flow in large vessels require appropriate techniques to avoid artificial wave reflections at those boundaries. In this perspective the geometrical multiscale approach can be regarded as a new method for solving a class of problems, whose application goes beyond those addressed in this book.

Despite the simplicity of the basic idea, the coupling of NS, E and K models lead to nontrivial problems at both the mathematical and the numerical level. After a quick review of geometrical multiscale models of the cardiovascular system and the coupling conditions based on some intuitive formulations, we will consider in more details the mathematical aspects of this approach, leading to less immediate and however more accurate solutions.

11.2 Setting up of geometrical multiscale models

A main issue of the geometrical multiscale modelling is to devise mathematically and physically sound coupling conditions among the models, and develop efficient techniques for their numerical computation.

11.2.1 Coupling of 3D and 1D models

According to the top-down approach introduced above, let us consider the coupling of 3D and 1D models for haemodynamics (see Fig. 11.2). This technique is of interest for instance when an endograft prosthesis or a stent is deployed in a specific district (abdominal aorta, carotid, etc.) and one is interested to the alterations induced by this operations on the pressure propagation over the vascular tree.

As already mentioned, this is also an effective way to implement physically based absorbing conditions, in particular for a 3D compliant model. As it has been pointed out in Chapter 3 (see also [155]) the solution of the fluid-structure interaction problem in a compliant vessel Ω_{3D} features a propagative behaviour, similar to that of a compressible flow in a rigid pipe. We have seen in the previous chapter that two pulse waves travel along the circulatory system, in opposite directions. The domain Ω_{3D} normally represents just a tiny portion of the whole cardiovascular system, for instance a specific artery. The pulse waves outgoing the artery are partially reflected by the remaining part of the system and give rise to a backward wave (see Chapter 10) which eventually re-enters the artery under consideration. Forward and backward components are related to the structure of vascular tree and their correct mathematical description is crucial to avoid artifacts in the numerical solution

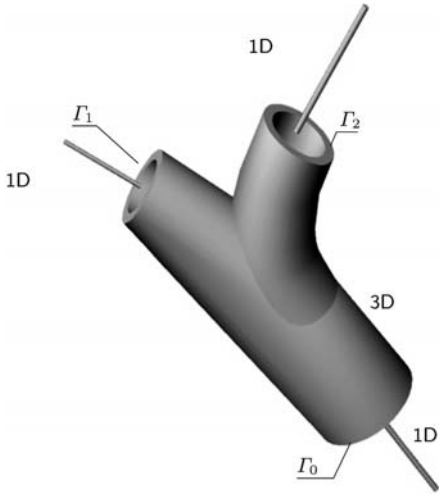

Fig. 11.2. A 3D-1D model

induced by a wrong decomposition of incoming and outgoing waves. Coupling of 3D and 1D models is a possible and reliable approach to achieve this goal and requires the introduction of a proper 1D representation of the vascular tree around Ω_{3D}.

Appropriate matching conditions drive the data exchange between NS and E models at the interface Γ (see Fig. 11.3). Different conditions in fact can be considered. In particular we refer to the following quantities defined on Γ (see [155])

$$\begin{aligned} A = \text{meas}(\Gamma), \quad Q = \int_\Gamma \boldsymbol{u} \cdot \mathbf{n} d\gamma, \\ \overline{\boldsymbol{u}} = \frac{1}{A}\int_\Gamma \boldsymbol{u} \cdot \mathbf{n} d\gamma = \frac{Q}{A}, \quad \overline{p} = \frac{1}{A}\int_\Gamma p d\gamma. \end{aligned} \tag{11.1}$$

A priori, it is reasonable to prescribe the continuity of the following quantities at the interface:

[A] area: $A_{3D} = A_{1D}$;
[B] mean pressure: $\overline{p}_{3D} = \overline{p}_{1D}$;
[C] flux: $Q_{3D} = Q_{1D}$;
[D] incoming characteristic: $\overline{\boldsymbol{u}}_{3D} + \dfrac{8}{\rho}\left(\sqrt{\overline{p} - p_{ext} + p^*} - \sqrt{p^*}\right) = W_{1,1D}$;
[E] mean total pressure: $\overline{p}_{3D} + \dfrac{1}{2}\overline{\boldsymbol{u}}^2_{3D} = \overline{p}_{1D}\dfrac{1}{2}\overline{\boldsymbol{u}}^2_{1D}$,

where $W_{1,1D}$ is the incoming characteristic variable[2] introduced in (10.37), p_{ext} is the pressure external to the vessel and p^* depends on the physical

[2] The incoming characteristic variable is W_1 because we are considering an interface which is an outflow (distal) boundary for the 3D model and correspondingly an

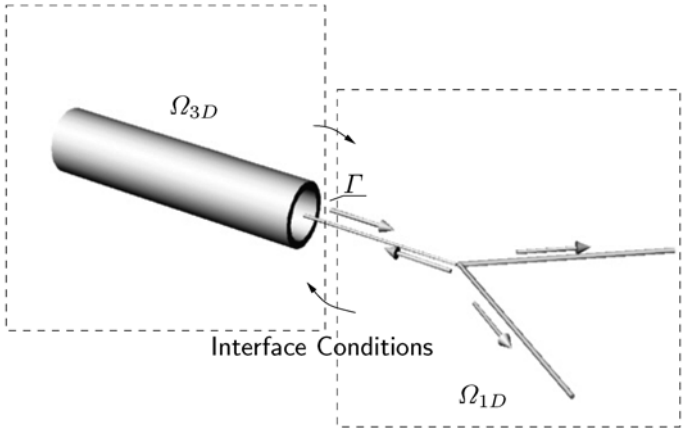

Fig. 11.3. 3D-1D model: detail of the coupling at the outflow of Ω_{3D}

features of vascular walls (see Chapter 3). The conditions above are not all independent. For instance, [A],[B] and [D] imply conditions [C]. Similarly, conditions [A], [C] and [D] imply [B]. Moreover, it is worth observing that, following the derivation of 1D models carried out in Chapter 10, conditions [B], [D] and [E] can be replaced by similar conditions where the mean pressure on the 3D side is replaced by the averaged normal stresses (see Chapter 3 and [155]), yielding:

[B1] $\overline{\sigma_{\mathbf{n}}}_{3D} = \overline{p}_{1D}$;
[D1] $\overline{\boldsymbol{u}}_{3D} + \dfrac{8}{\rho}\left(\sqrt{\overline{\sigma_{\mathbf{n}}} - p_{ext} + p^*} - \sqrt{p^*}\right) = W_{1,1D}$;
[E1] mean total pressure: $\overline{\sigma_{\mathbf{n}}}_{3D} + \dfrac{1}{2}\overline{\boldsymbol{u}}^2_{3D} = \overline{p}_{1D}\dfrac{1}{2}\overline{\boldsymbol{u}}^2_{3D}$.

In practise, we can identify different (alternative) sets of independent interface conditions:

a) [A], [B], [D];
b) [A], [C], [D];
c) [A], [B1], [D1];
d) [A], [C], [D1];
e) [A], [E], [D];
f) [A], [E1], [D].

Different possible choices that are equivalent form the mathematical viewpoint can however lead to different numerical schemes.

inflow (proximal) boundary for the 1D model. Should we swap the sequence of 1D and 3D models, the incoming characteristic variable would be W_2.

Some numerical issues

In numerical solution of multiscale models presented above it is natural to split the scheme into the iterative sequence of dimensionally homogeneous problems, namely 3D and 1D separately. In this way, we can figure out for instance the following algorithm to be carried out at each time step[3]. We focus our attention on interface between the two models. In particular, we refer to interface conditions (b) of the previous list. The conditions on the other boundaries are assumed to be standard (see Chapter 3 and 10).

`Initialisation.` Set $k = 0$ and select an initial guess for the mean velocity $\overline{\boldsymbol{u}}_{3D}^{(0)}$ and pressure $\overline{p}^{(0)}$ at the interface. Typically, this guess is given by the same quantities at the end of the previous time step.

`Loop.`

1. *Solve* the 1D model, using [D] as boundary condition at the interface, by computing $W_1^{(k)}$ as a function of the current guess of the mean velocity and pressure (or normal stress). The other boundaries of the 1D model will be properly managed (see Section 10.1.5). In this step, $A_{1D}^{(k+1)}$ and $Q_{1D}^{(k+1)}$ are computed.
2. *Solve* the 3D fluid-structure interaction model, with [A] as a boundary condition for the structure and [C] for the fluid by using $A_{1D}^{(k+1)}$ and $Q_{1D}^{(k+1)}$. At the end of this step, compute the new guess $W_1^{(k+1)}$. Set $k = k + 1$.

`Test.` The loop ends when:

$$|W_1^{(k)} - W_1^{(k-1)}| \leq \varepsilon, \quad |A^{(k)} - A^{(k-1)}| \leq \varepsilon, \quad |Q^{(k)} - Q^{(k-1)}| \leq \varepsilon \tag{11.2}$$

being ε a given tolerance.

Analogous algorithms can be devised for the other interface conditions.

While the boundary conditions in step (1) of the loop lead to a mathematically well posed problem, step (2) in this form does not, since these averaged data on the boundary are not enough to guarantee uniqueness of solution for the associated 3D problem. A specific treatment of these problems is required. To be more concrete, let us use condition [A] for the structure at step 2. On the 3D compliant model we would need pointwise data for the wall displacement $\boldsymbol{\eta}$. On the other hand, when the area of the interface $\Gamma(t)$ is known from the computation of the 1D model, we have the average condition:

$$\int_{\Gamma(t)} d\gamma = A_{1D}(t). \tag{11.3}$$

We need to "spread" the average data to pointwise conditions on the displacements $\boldsymbol{\eta}$. To this aim we can assume a shape for the displacement depending

[3] We will not put in evidence explicitly the temporal level for the sake of notation.

on a single parameter to be tuned so to force (11.3). For instance, assume that Γ is circular with centre on the axis of coordinates (x_c, y_c, z_c), and belongs to the plane identified by the equation $z = z_c$. In this way the component η_3 along z of $\boldsymbol{\eta}$ is constant and equal to zero and we can set:

$$\eta_1(x, y, z, t) = \Delta R(t) \cos\left(\tan^{-1}\left(\frac{y}{x}\right)\right) = \sqrt{\frac{A_{1D}(t) - A_0}{\pi}} \cos\left(\tan^{-1}\left(\frac{y}{x}\right)\right),$$
$$\eta_2(t) = \Delta R(t) \sin\left(\tan^{-1}\left(\frac{y}{x}\right)\right) = \sqrt{\frac{A_{1D}(t) - A_0}{\pi}} \sin\left(\tan^{-1}\left(\frac{y}{x}\right)\right). \tag{11.4}$$

Here A_0 is the reference area of section Γ, corresponding to a zero displacement, and $\Delta R(t) = R(t) - R_0$ is the difference between the current and the reference radius. With this choice the average condition has been extended to pointwise data by assuming a priori a planar circular shape for the interface Γ. This technique can be extended to more general shapes.

In a similar way we can address condition [C], by assuming, for instance, a velocity profile depending on a single parameter. For instance, let us assume again that Γ has a circular shape in the $xy-$plane. Then, we can resort to the Poiseuille velocity field (see Chapter 5):

$$u_1 = u_2 = 0, \quad u_3(x, y, t) = \frac{2Q_{1D}(t)}{\pi\rho R^2}\left(1 - \frac{(x - x_c)^2 + (y - y_c)^2}{R^2}\right), \tag{11.5}$$

where Q_{1D} is the flow rate computed by the 1D model. Again, the arbitrary selection of a velocity profile converts the average conditions into pointwise Dirichlet conditions for the fluid problem.

Numerical results (see Fig. 11.4 and 11.5) show that this approach is actually able to reduce spurious back-reflections at the boundaries, in particular when the arbitrary assumptions on the displacement shape or the chosen velocity profile are realistic. However, in general, the arbitrary selection of a shape for the displacement or the velocity profile strongly affects the numerical solution. Hence, the reliability of results obtained in this way is sometimes questionable. More sophisticated mathematical and numerical techniques that are able to expand average data to pointwise conditions are required for ensuring better accuracy. We will address these techniques in Section 11.3.

Another drawback of this multiscale coupling still relies on the limited capability of E models of covering the capillary network, which on the other hand is the main source of the back reflections propagating in the arterial tree and of including the action of the heart. More sophisticated multiscale models are therefore needed.

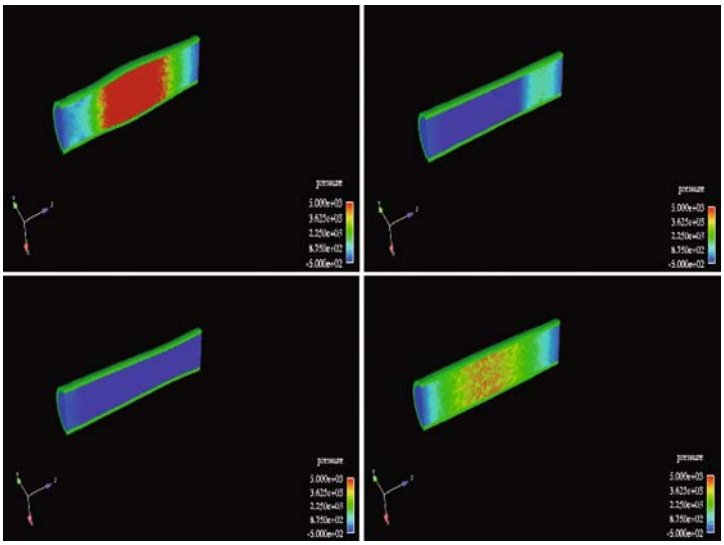

Fig. 11.4. 3D simulation: pressure wave propagation along a compliant vessel. Spurious effects arise at the artificial downstream boundary

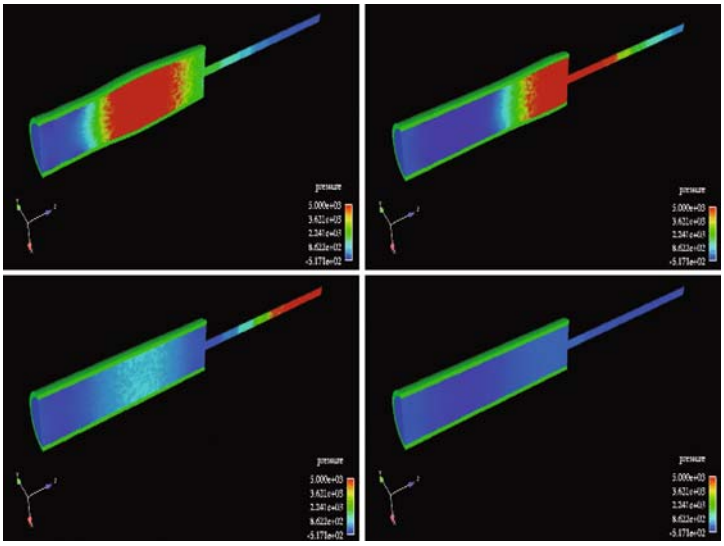

Fig. 11.5. Multiscale 3D-1D simulation: pressure wave propagation along the two submodels. Spurious effects at the artificial boundary are small

11.2.2 Coupling of 1D-0D and 3D-1D-0D models

A possible way to account for the presence of the capillary bed and the action of the heart is to close the 3D-1D network with K models. This requires in particular the coupling of 1D and lumped parameter models, through interface conditions. A simplified version of this coupling has been already addressed in Chapter 10. In that case, lumped parameter models were represented by a simple terminal impedance for prescribing boundary conditions in the frequency domain at the downstream sections of a 1D network. Here, we want to give an insight of models and numerical issues arising from a precise and accurate inclusion of the dynamics in K models. In the multiscale framework they are described in terms of a system of differential-algebraic equations (DAE – see (10.84)) in the time variable.

For the sake of simplicity, we consider the multiscale model represented in Fig. 11.6, where the 1D model represents a simple cylindrical domain. More complex problems, featuring a network of 1D segments or even a coupled 3D-1D model can be considered as well within the same framework.

In the model at hand we have two interfaces, Γ_0 and Γ_1, where it is reasonable to prescribe the continuity of:

[A] area: $A_{1D} = A_{0D}$;
[B] pressure: $P_{1D} = P_{0D}$;
[C] flow rate: $Q_{1D} = Q_{0D}$.

Moreover, we could require the continuity of the Riemann variables:

[D] characteristic variable propagating from the heart to the peripheries:
$$\frac{Q_{0D}}{A_{0D}} + \frac{8}{\rho}\left(\sqrt{P_{0D} - p_{ext} + p^*} - \sqrt{p^*}\right) = W_{1,1D};$$
[E] characteristic variable propagating from the peripheries to the heart:
$$\frac{Q_{0D}}{A_{0D}} - \frac{8}{\rho}\left(\sqrt{P_{0D} - p_{ext} + p^*} - \sqrt{p^*}\right) = W_{2,1D}.$$

Again, these conditions are not all independent. This is the case for instance of [A] and [B], since both the E and K models include a wall law linking together pressure and area. Should these wall laws be the same, the continuity of the area would imply the continuity of the pressure and vice-versa. More in general, only one between [A] and [B] can be explicitly prescribed.

Similarly, only two conditions among [B], [C], [D] and [E] can be selected, for instance:

1. conditions [B], [D] at the upstream interface Γ_0;
2. conditions [C], [E] at the downstream interface Γ_1.

Some numerical issues

A possible approach for solving this multiscale model still resorts to splitting the computation into the sequence of dimensionally homogeneous problems.

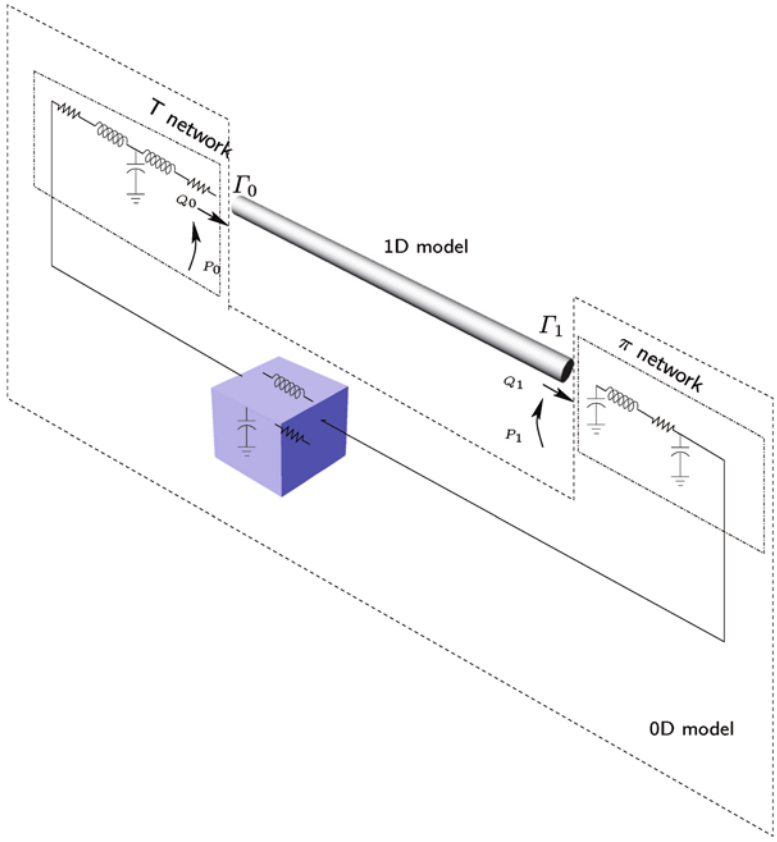

Fig. 11.6. 1D-0D model: the 1D model is given by a simple compliant straight cylinder, the 0D model is composed by the network in the cube and two bridging regions (upstream and downstream). Upstream bridging region is given by a T network, featuring the flow rate Q_0 as state variable. Downstream bridging region has the pressure P_1 as state variable. These interface compartments are compatible with the splitting scheme described in the text

In the case of Fig. 11.6, this means that we solve separately the DAE system arising from the lumped parameter model and the Euler hyperbolic system. Let us consider preliminarily the simple case in which a 1D straight cylinder is split into a 1D-0D model as illustrated in Fig. 11.7. In particular, let us consider the multiscale model at the top of Fig. 11.7, where the 0D model is represented by a $\mathcal{L}$ inverted network (see Chapter 10). The lumped parameter model is therefore described by the following equations:

$$\begin{aligned} C\frac{dP}{dt} &= Q_{up} - Q, \\ L\frac{dQ}{dt} + RQ &= P - P_{dw}. \end{aligned} \tag{11.6}$$

A possible iterative scheme reads as follows. At each time step:

`Initialisation.` Set $k = 0$ and fix an initial guess for the interface flow rate $Q_{up}^{(0)}$.

`Loop.`

1. *Solve* the 0D model (11.6), by using $Q_{up}^{(k)}$ as forcing term. This yields the estimates of $Q^{(k)}$ and $P^{(k)}$. On the basis of this computation, Riemann variable $W_2^{(k)}$ at the interface entering the 1D model can be computed.
2. *Solve* the 1D model by using incoming Riemann variable $W_2^{(k)}$ as boundary condition. At the end of this step, a new guess for $Q_{up}^{(k+1)}$ is available. Set $k = k + 1$.

`Test.` The loop ends when the solution fulfils an appropriate test, for instance:

$$|P^{(k)} - P^{(k-1)}| \leq \varepsilon, \quad |Q_{up}^{(k)} - Q_{up}^{(k-1)}| \leq \varepsilon.$$

Let us consider now the multiscale model on the bottom of Fig. 11.7. Here 0D model is represented by a $\mathcal{L}$ network, described by system

$$\begin{aligned} L\frac{dQ}{dt} + RQ &= P_{up} - P, \\ C\frac{dP}{dt} &= Q - Q_{dw}. \end{aligned} \tag{11.7}$$

We can still use an iterative approach as follows.

`Initialisation.` Set $k = 0$ and fix an initial guess for interface pressure $P_{up}^{(0)}$.

`Loop.`

1. *Solve* the 0D model (11.7), by using $P_{up}^{(k)}$ as forcing term. This yields the estimates of $Q^{(k)}$ and $P^{(k)}$. On the basis of this computation, Riemann variable $W_2^{(k)}$ at the interface entering the 1D model can be computed.
2. *Solve* 1D model by using incoming Riemann variable $W_2^{(k)}$ as boundary condition. At the end of this step, a new guess for $P_{up}^{(k+1)}$ is available. Set $k = k + 1$.

`Test.` The loop ends when the solution fulfils an appropriate test, for instance:

$$|P_{up}^{(k)} - P_{up}^{(k-1)}| \leq \varepsilon, \quad |Q^{(k)} - Q^{(k-1)}| \leq \varepsilon.$$

Several remarks are in order. First of all the use of characteristic variables has the advantage of prescribing (at least approximately) absorbing boundary conditions, well suited for avoiding numerical reflections at the boundary of the E model (see Chapter 10).

Secondly, interface conditions are by definition localised in a specific position in space. On the other hand, K models have lost an explicit space dependence. Therefore, in managing matching conditions with K models:

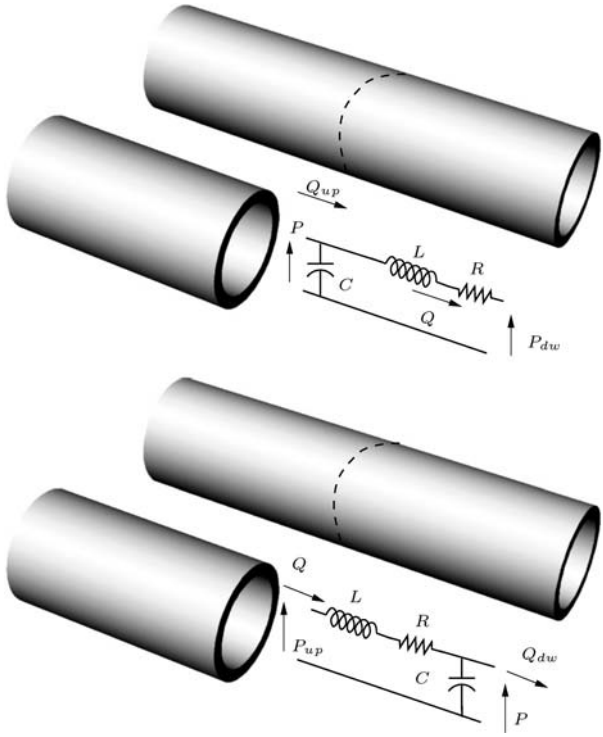

Fig. 11.7. Two simple examples of 1D-0D multiscale models. At the top, the lumped parameter model is given by a $\mathcal{L}$-inverted network. On the bottom, it is given by a $\mathcal{L}$ network. The two network configurations are appropriate for different iterative solvers (see text)

1. interface conditions yield a forcing term in the 0D model;
2. different configurations of the 0D models are associated with different iterative schemes: in the first case the 0D model is forced by the flow rate Q_{up} and provides the pressure P; in the latter case, it is forced by the pressure P_{up} and provides the flow rate Q.

The latter item deserves some further remarks. In lumped parameter problems, interfaces between E and K models are represented by the boundary of the 1D domain and the compartments placed in the neighbourhood of the 1D models[4]. The type of network used in these compartments defines implicitly the state variables and forcing terms for the 0D model. In an iterative scheme, the latter will be provided to the 0D model by the 1D problem, while the former are the variables that will be computed by the 0D and used to build the boundary condition for the 1D model.

[4] In the two oversimplified examples above they in fact corresponds to the entire 0D models.

We call *bridging regions* those compartments of the 0D model that play the role of the interfaces with the other models. The link between the graph of the bridging regions and the numerical scheme will be called *bridging region compatibility* (see [409]). More precisely, we say that a numerical scheme is *bridging region compatible* if it is consistent with the topology of the bridging regions.

For instance, for the multiscale model of Fig. 11.6, where the upstream bridging region is given by a T network and the downstream one is given by a π network, a bridging region compatible scheme reads as follows.

`Initialisation.` Set $k = 0$ and fix an initial guess for the upstream pressure $P_0^{(0)}$ and the downstream flow rate $Q_1^{(0)}$.

`Loop.`

1. *Solve* the 0D model, by using the available upstream pressure and the downstream flow rate as forcing terms. Compute in particular the upstream flow rate $Q_0^{(k)}$ and the downstream pressure $P_1^{(k)}$. After this computation, the incoming characteristic variables, $W_1^{(k)}$ upstream and $W_2^{(k)}$ downstream are available.
2. *Solve* the 1D model by using the incoming characteristic variables as boundary conditions. At the end of this step, new guesses for the upstream pressure $P_0^{(k+1)}$ and the downstream flow rate $Q_1^{(k+1)}$ are available.

`Test.` The loop ends when the solution fulfils an appropriate test, for instance:

$$|P_i^{(k)} - P_i^{(k-1)}| \leq \varepsilon, \quad |Q_i^{(k)} - Q_i^{(k-1)}| \leq \varepsilon, \qquad i = 0, 1.$$

Remark 11.2.1 *Step 1 can be regarded as a stand-alone lumped parameter model, represented by the circuit of Fig. 11.8, where input variables of the 1D model are represented by a current and a voltage generator respectively. In terms of circuit analysis bridging region compatibility in fact implies that no voltage/pressure generator is in parallel with a capacitor and no current/flow rate generator is in series with an inductance. Under these assumptions it is possible to prove that the DAE system associated with this stand-alone network is of index 1 and it can be reduced to a well posed Cauchy problem for a system of ordinary differential equations (see [121, Chap. 12]).*

Aortic valve function

As we have pointed out, an advantage of K models is their capability of representing in relatively simple terms complex systems like the heart or the action of control dynamics. Moving from the observation that "the left ventricle and arterial circulation represent two mechanical units that are joined together to form a coupled biological system" [350, Chap. 13], it makes sense to consider a 1D model for the aorta coupled with the lumped parameter model of the

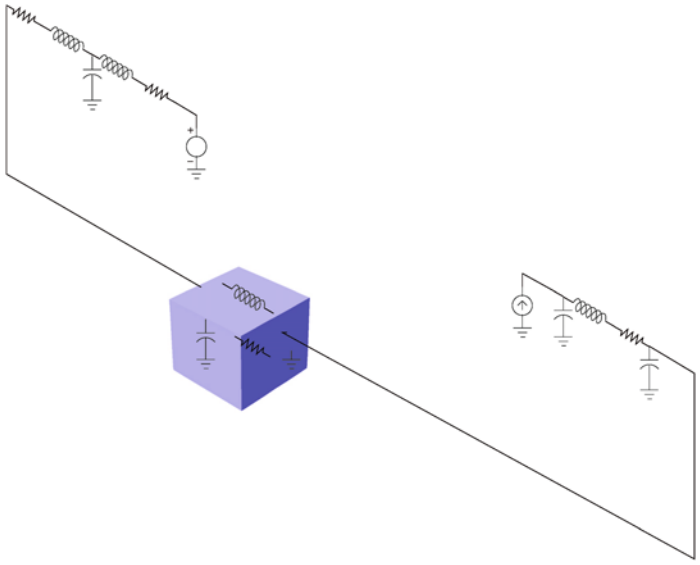

Fig. 11.8. Stand alone 0D model corresponding to step 2 of the splitting iterative algorithm (see text)

heart presented in Section 10.2.1. Since the coupling is mediated by the aortic valve, we assume that there are two possible working states for the system Heart-Aorta.

1. *Closed valve (CV) condition*: when the aortic valve is closed, the two systems are actually decoupled; in particular, for the arterial tree we have a null flow rate condition at the aorta inflow, which in terms of the characteristic variables implies
$$W_1 = -W_2.$$
2. *Open valve (OV) condition*: the ventricular pressure is related to the 1D problem by solving equation (10.82) which we recall here for the sake of clarity:
$$\frac{1}{E_v}\frac{dP_v}{dt} + \frac{d}{dt}\left(\frac{1}{E_v}\right)P_v = -Q_v.$$
During this phase, we assume that ventricular flow rate Q_v and pressure P_v are equal to the arterial ones at the aorta inflow (see Fig. 11.9), corresponding to conditions
$$Q_v = Q_{1D}, \quad P_v = P_{1D}.$$
A numerical implementation of these conditions by using the incoming characteristic variable in the 1D network is addressed in [158].

Transition between OV and CV conditions cannot be prescribed a priori. We assume that the valve opens under the action of a differential pressure

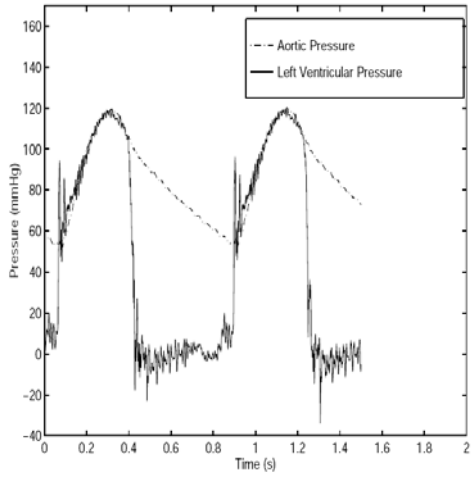

Fig. 11.9. Ventricular and arterial pressures during the heart beat. When the aortic valve is open, the two pressures can be assumed to be the same

and it closes when forced by a flow reversal. This means that when the valve is closed we need to compare at each time step the aortic and ventricular pressure. If $P_v - P_{1D} < 0$ the valve is kept closed (CV conditions), otherwise we switch to the OV conditions until the next closure. To determine the instant of valve closure (end of systole) we check the sign of the flux at the aortic proximal node. At the first time step when Q_v becomes negative we "close" the valve by adopting again CV boundary condition, up to the next heart cycle (see Fig. 11.10).

In [158] this multiscale model has been used for simulating a 1D network of the largest 55 arteries, coupled with the heart. The microcirculation is represented by simple Windkessel models at every 1D terminal section. Figure 11.11 pinpoints the relevance of the multiscale model (right column) in comparison with a standard approach, in which the action of the heart is described as a boundary condition, not sensible to the real functioning of the arterial network. The standard model actually damps wave reflection, in particular in the pathological case in which right femoral artery is supposed to be surgically closed.

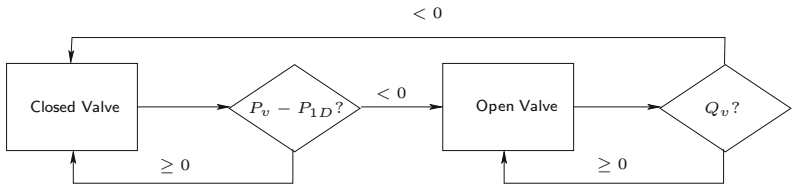

Fig. 11.10. Flow chart representation of the aortic valve modelling

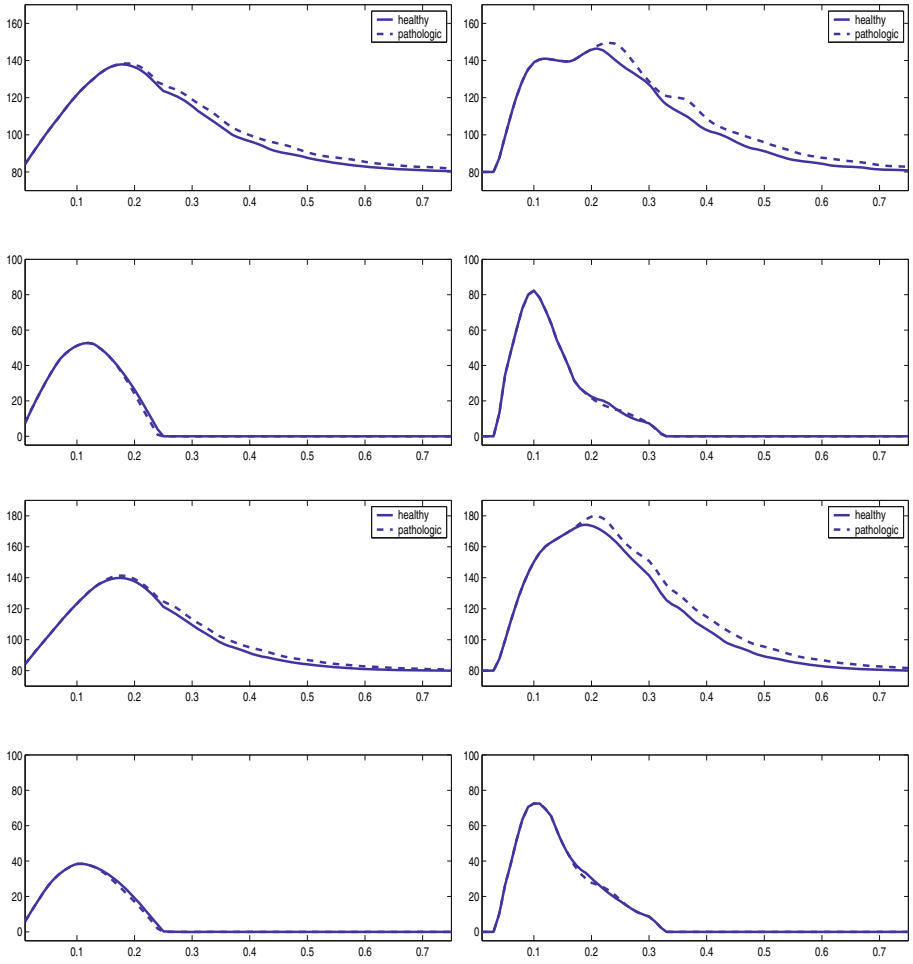

Fig. 11.11. Comparison between the results obtained with standard proximal conditions (left) and the coupling with the ventricular model (right). Values of velocity (first and third rows) and pressure (second and fourth rows) in the mid-point of the aorta are presented. We have simulated circulation in a physiologic (solid) and pathologic (dotted) test case. The pathologic case corresponds to a total occlusion of the right femoral artery. The first two rows refer to an adult patient, the other ones to an elder patient. Pictures taken from [158], reproduced with permission

11.2.3 Coupling of 3D-0D models

In our top-down approach, we have coupled the three kind of models, moving from the finest 3D down to the coarsest 0D. In some applications a sort of *shortcut modelling* can be pursued, coupling together directly 3D and 0D models. This is, for instance, the case when the wave propagation phenomena

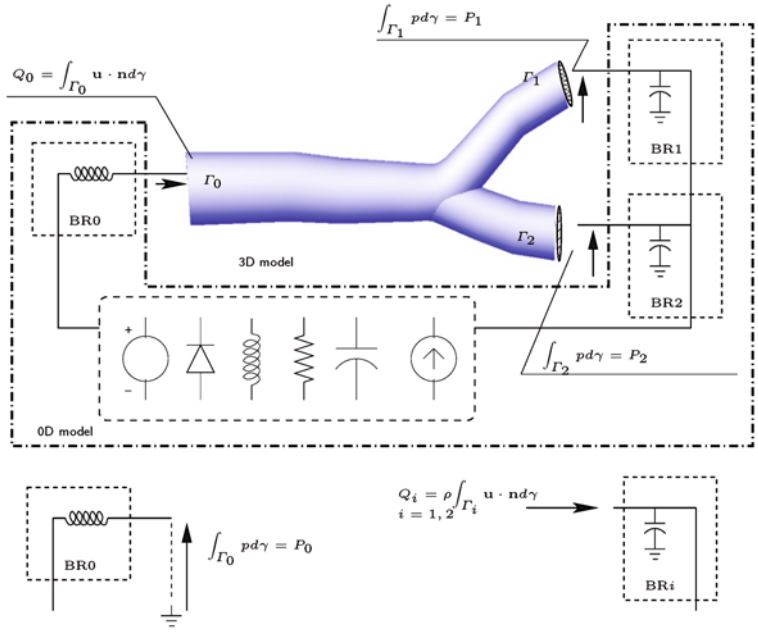

Fig. 11.12. Representation of a 3D rigid-0D geometrical multiscale model with three bridging regions (BR0, BR1, BR2). At the inlet of the 3D domain, the bridging region has the current/flow rate Q_0 as state variable. The latter is computed by the 0D model and provided to the NS model. In the other bridging regions, the voltage/pressures p_i, $i = 1, 2$, are the state variables. The 0D model is forced by the mean pressure at the interface Γ_0 and by the flow rates at Γ_1 and Γ_2

are not of interest, and a 3D simulation needs boundary conditions that could account in a precise way the dynamics of the complete vascular tree. An example of clinical relevance of this situation is given in Chapter 12.

Consider for instance the model obtained by coupling a 3D model of a region of interest and a lumped parameter model like in Fig. 11.12. Again, three model ingredients can be identified:

K model, represented by a system of ordinary differential equations in the form

$$\frac{d\mathbf{y}}{dt} + A\mathbf{y} = \mathbf{f}.$$

NS model, represented by the Navier-Stokes equations with appropriate boundary conditions on the vascular walls Γ_w;

interface conditions represented by continuity conditions.

In particular, at each interface we consider the following conditions:

[A] area: $A_{3D,i} = \text{meas}(\Gamma_i) = A_{0D,i}$;

[B] mean pressure: $\overline{p}_{3D,i} = \dfrac{1}{A_{3D,i}} \displaystyle\int_{\Gamma_i} pd\gamma = P_{0D,i}$;

[C] flow rate: $Q_{3D,i} = \rho \int_{\Gamma_i} \boldsymbol{u} \cdot \mathbf{n}_i d\gamma = Q_{0D,i}$.

As we have already pointed out for the 3D-1D coupling, condition [B] can be replaced by a condition on the normal component of the stress

[B1] $\dfrac{1}{A_{3D,i}} \displaystyle\int_{\Gamma_i} (p\mathbf{n}_i - (\nabla \mathbf{u} + \nabla \mathbf{u}^T) \cdot \mathbf{n}_i) d\gamma = P_{0D,i}$.

Possible interface conditions are therefore represented by [A], [B] and [C], or else by [A], [B1] and [C]. If the 3D model is assumed to be rigid, the three conditions are not independent and in particular [A] and [B] (or [B1]) cannot be prescribed together. Actually, in the 3D model the area at the interface is constant, while in the 0D model is not. Indeed it is related to the pressure by an algebraic law like (10.21). For this reason, typical interface conditions in the 3D rigid-0D coupling are [B] (or [B1]) and [C].

Some numerical issues

We consider the problem represented in Fig. 11.12 where the 3D model is assumed to be rigid and interface conditions [B1] and [C] are prescribed. We consider the following algorithm for the numerical coupling at each time step.

`Initialisation.` Select an initial guess for the pressure $P_0^{(0)} = P_0$ and the flow rates $Q_1^{(0)} = Q_1$ and $Q_2^{(0)} = Q_2$ at the interfaces. Typical choice is to take these quantities from the previous time step. Set the iteration index $k = 0$.

`Loop.`

1. *Solve* the 0D model by using the forcing terms $P_0^{(k)}$, $Q_1^{(k)}$ and $Q_2^{(k)}$. This step, in particular, computes the state variables of the K model $Q_0^{(k+1)}$, $P_1^{(k+1)}$ and $P_2^{(k+1)}$.
2. *Solve* the 3D model by using the boundary conditions given by $Q_0^{(k+1)}$, $P_1^{(k+1)}$ and $P_2^{(k+1)}$. Compute the average normal stress on Γ_0, $P_0^{(k+1)} = \int_{\Gamma_0} (p^{(k+1)}\mathbf{n}_0 - (\nabla \mathbf{u}^{(k+1)} + \nabla \mathbf{u}^{(k+1),T}) \cdot \mathbf{n}_0) d\gamma$ and the flow rates $Q_i^{(k+1)} = \rho \int_{\Gamma_i} \mathbf{u}^{(k+1)} \cdot \mathbf{n}_i d\gamma$, for $i = 1, 2$.

`Test.` The iteration continues up to the fulfilment of a convergence test, for instance:

$$|P_i^{(k+1)} - P_i^{(k)}| \leq \varepsilon, \qquad |Q_i^{(k+1)} - Q_i^{(k)}| \leq \varepsilon, \quad i = 0, 1, 2.$$

As done previously, several remarks are in order.

1. *Bridging region compatibility.* The compartment that stands at the interfaces with the 3D model (bridging region) has to be devised appropriately. More precisely, it should allow the calculation of the quantities required by the splitting scheme. For instance, in the example presented in Fig. 11.12

the flow rate on Γ_0 and the pressures P_1 and P_2 on Γ_1 and Γ_2, respectively, must be state variables of the lumped parameter model. As we have pointed out, this ensures well posedness of the problem solved at step 1.

2. *3D defective boundary data problems.* The K model (as well as the E model) computes averaged quantities that do not provide enough boundary data to the 3D model in step (2) of the loop. As for the coupling between 3D and 1D models, we could postulate a priori single parameter profile for the velocity or the normal stress and use the average data to set the parameter appropriately. For instance, we could "expand" average data into pointwise data in the following manner:

   Flow rate conditions $\rightarrow$ Poiseuille parabolic profile $\rightarrow$ (Standard) Dirichlet conditions (see (11.5));

   Average pressure conditions $\rightarrow$ Constant normal stress $\rightarrow$ (Standard) Neumann conditions:

$$p\mathbf{n} - \nu\nabla\boldsymbol{u}\cdot\mathbf{n} = P\mathbf{n} \tag{11.8}$$

   where P is constant over the interface.

   At which extent numerical results are affected by this arbitrary profile selection is a crucial question for the reliability of multiscale modelling. We will address this problem in the next sections.

Fig. 11.13 illustrates some numerical results with a multiscale model (2D coupled with a 0D model) with the aim of computing the flow distribution in a by-pass anastomosis for different levels of occlusions in the stenotic vessel (results taken from [402]). This distribution strongly depends on the behaviour of the whole vascular system. Consequently, the multiscale 3D-0D coupling is an appropriate numerical tool for investigating the effectiveness of the by-pass.

Remark 11.2.2 *The same algorithm for the 3D-0D coupling can be extended to the compliant case. If the 3D compliant model adopts an algebraic model for the vascular walls, no further interface conditions are needed. In the case of a differential (in space) structure model, conditions on the displacements should be prescribed. Again, as we have seen in the 3D-1D coupling, a condition on the section area is not enough for the structure problem. A workaround is to expand it into a pointwise Dirichlet condition as we have done in (11.4).*

11.2.4 Improving multiscale models

So far, we have proposed different coupled models, with some basic ideas for their numerical implementation. A mismatch of mathematical characteristics of the submodels we want to couple requires specific strategies to obtain feasible and efficient multiscale simulations. In particular, we have already outlined the role of the characteristic variables as interface conditions in the coupling of E models. They allow to formulate absorbing boundary conditions for the E model, allowing a better description of wave propagation dynamics at the interface. Another crucial issue is the role played by bridging regions in coupling with K models.

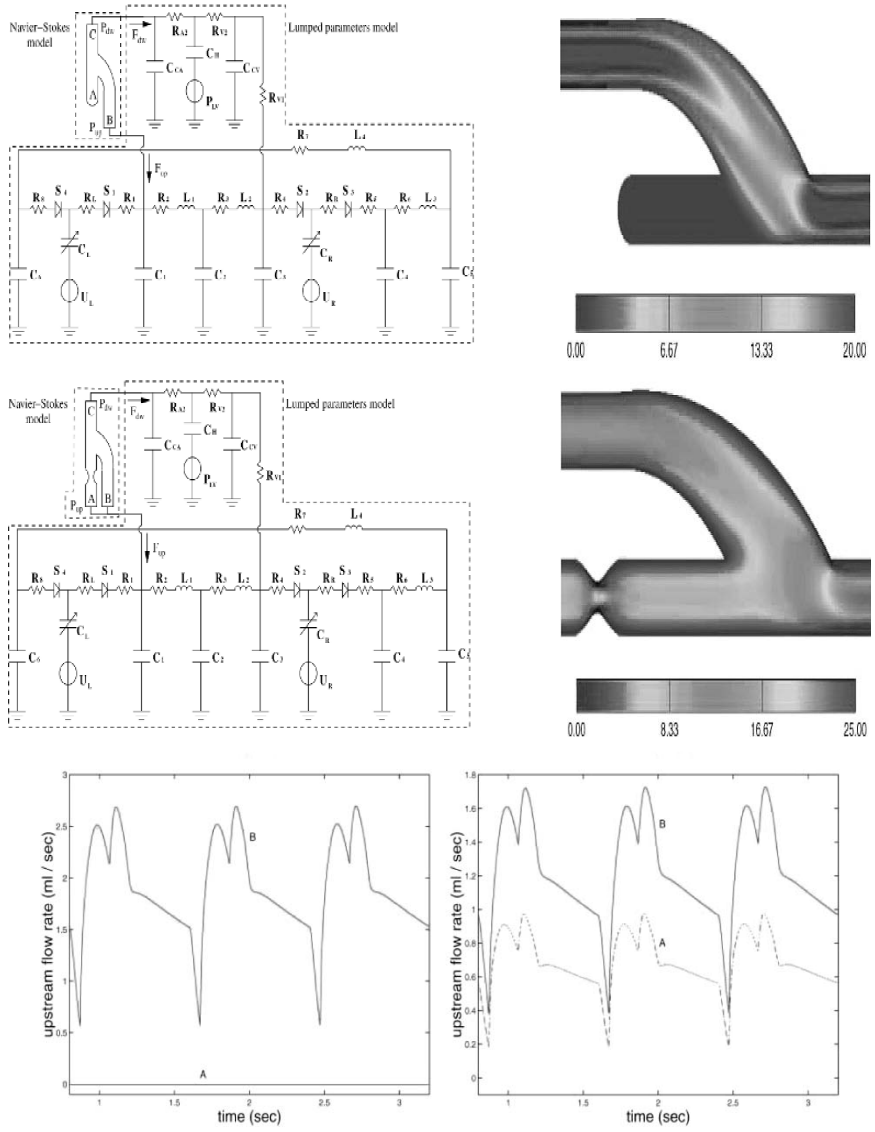

Fig. 11.13. Top: Left, multiscale problem with a completely occluded host artery and a by-pass; Right: results in the fine domain at the end of a heart beat. Centre: as in the Top line, but for a partially occluded case. Bottom: Flow division in the host artery and in the graft for the two cases. On the left, the completely occluded case. On the right, the partially occluded case. Pictures taken from [402]

There are two further issues that deserve a further investigation, for the improvements of multiscale modelling.

Average data expansion: when coupling 3D with 1D or 0D models, we need to convert average data into proper boundary conditions for a differential problem that requires "pointwise data" instead. We have proposed some practical strategies, which however introduce a level of arbitrariness in the final numerical solution. Indeed, numerical results in [342, 527] show how the prescription of an arbitrary velocity profile can sometimes induce incorrect results (and maybe lead a medical researcher to wrong conclusions). We need therefore to understand if there is an optimal approach able to reduce the impact on the final solution of the unavoidable arbitrariness. To be more precise, if we select an arbitrary parabolic profile at the inlet of a cylindrical pipe, as done in (11.5), we could expect that this choice will not affect the numerical results far away from that inlet boundary. This "entry problem" has been studied mathematically and a review of the theory and main results may be found in [181]. In practise, for steady problems and in conditions akin to that in the cardiovascular system, it is commonly accepted that the effects of the profile chosen at the inlet are no more significant after an entry length $L \approx 0.06D$ where D is the diameter of the pipe (see [542]). However, for unsteady problems it has been verified in [423] that an entry length of $40D$ may be not enough to recover the analytical (Womersley) solution from a prescription of an inlet parabolic profile. Different strategies, able to force a given flow rate *without* the prescription of a velocity profile are then necessary to improve the reliability of multiscale results.

Efficiency of coupling iterative schemes: we have presented some basic iterative schemes, resorting to the successive solution of standard subproblems. The effectiveness of this kind of schemes (in terms of number of iterations required for the convergence) can be improved for instance by introducing appropriate relaxation strategies. Convenience of such splitting schemes in comparison with non-splitting or monolithic solvers is another relevant point in devising multiscale models.

We investigate these two items in the next sections. We also discuss mathematical well posedness of multiscale models.

11.3 Defective boundary data problems

Let us consider the 3D Navier-Stokes equations (see Chapter 2):

$$\begin{aligned} &\rho\frac{\partial \boldsymbol{u}}{\partial t} + \rho\boldsymbol{u}\cdot\nabla\boldsymbol{u} - \mu\triangle\boldsymbol{u} + \nabla P = \mathbf{f}, \\ &\operatorname{div}\boldsymbol{u} = 0, \end{aligned} \tag{11.9}$$

that we assume to hold in the 3D domain Ω. The boundary $\partial\Omega$ still consists of the vascular wall Γ_w and the artificial boundaries Γ_i, with $i = 1, 2, \ldots, m$. For the time being, we assume that the vessel is rigid, i.e.

$$\boldsymbol{u}|_{\Gamma_w} = \mathbf{0}, \tag{11.10}$$

where Γ_w denotes the part of the boundary corresponding to the vascular wall. The initial conditions

$$\boldsymbol{u}(\boldsymbol{x}, 0) = \boldsymbol{u}_0(\boldsymbol{x}) \tag{11.11}$$

are assigned.

We will consider the two kind of averaged data encountered in the previous section, namely conditions on mean velocity or flow rates and on mean pressures.

11.3.1 Flow rate problem

Consider problem given by (11.9), (11.10), (11.11), together with boundary conditions:

$$\rho \int_{\Gamma_i} \boldsymbol{u} \cdot \boldsymbol{n} \, \mathrm{d}\boldsymbol{\gamma} = Q_i, \quad i = 0, 1, \ldots, m,$$

where Q_i are given functions of time. In the case of a rigid domain, the incompressibility of the fluid implies the following constraint on the data:

$$\sum_{i=0}^{m} Q_i = 0.$$

To avoid dealing with this constraint we will consider a slightly different problem, namely

$$P\boldsymbol{n} - \nu \frac{\partial \boldsymbol{u}}{\partial \boldsymbol{n}} = \mathbf{0}, \text{ on } \Gamma_0, \qquad \rho \int_{\Gamma_i} \boldsymbol{u} \cdot \boldsymbol{n} \, \mathrm{d}\boldsymbol{\gamma} = Q_i, \quad i = 1, \ldots, m. \tag{11.12}$$

In the analysis of this problem, we will prove however that there is no loss of generality with these conditions.

In the sequel, for the sake of simplicity, we set $\rho = 1$.

We have already pointed out that conditions (11.12) are not enough to guarantee the existence of a solution. Three scalar conditions should be required for the well posedness of the problem, while (11.12) provides only a scalar value for each Γ_i, for $i = 1, 2, \ldots m$. The approach advocated in the previous section was based on a-priori selection of a velocity profile fitting the given flow rate (see for instance [72, 151]).

This approach is in fact pretty simple, since it actually reduces the defective boundary problem to a classical Dirichlet one. Nevertheless there are several limitations. Real geometries (see e.g. Chapter 4) are typically far from

being cylindrical circular and rectilinear, which are the assumptions for the Womersley and Poiseuille solutions. Moreover, a-priori selection of a profile may affect the entire numerical solution.

In general, a practical workaround is to expand the computational domain (flow extensions), so that the arbitrary velocity profile is prescribed far away from the zone of interest. The downstream section of the extension is often made circular to apply a parabolic profile. However, this technique affects the computational costs, in particular for unsteady computations where, as we have pointed out, we need a rather long extension to damp out the effects of the arbitrary choice of the velocity profile.

Different approaches that do not require arbitrary prescription of a velocity profile are therefore very helpful.

A variational approach

A strategy proposed in [218] relies on the selection of an appropriate variational formulation for the problem at hand including all the available data. Variational formulation by itself will complete the boundary data set with homogeneous natural conditions. These conditions have been called sometimes *do nothing conditions*, since they are obtained spontaneously as a result of the chosen variational formulation[5]. They are indeed less perturbing (or "invasive") on the (unknown) solution, since they are natural conditions for the chosen variational formulation.

To introduce this approach for the flow rate problem, we need some functional spaces and a specific notation. Set:

$$\widehat{\mathbf{V}}_f \equiv \left\{ \mathbf{v} \in \boldsymbol{V}_f : \int_{\Gamma_j} \mathbf{v} \cdot \boldsymbol{n} = 0,\ \forall j = 1, 2, \ldots, m \right\},$$

and let us denote by $\mathbf{b}_i$, $i = 1, \ldots, m$ the functions of $\boldsymbol{V}_f$ such that, for all $j = 1, \ldots, m$

$$\int_{\Gamma_j} \mathbf{b}_i \cdot \boldsymbol{n}\, d\gamma = \delta_{ij}, \qquad \nabla \cdot \mathbf{b}_i = 0.$$

These functions are commonly called *flux carriers* and act as a lifting of the flow rate data. We set $\boldsymbol{u} = \widehat{\boldsymbol{u}} + \sum_{i=1}^{m} Q_i \mathbf{b}_i$. A possible variational formulation of the flow rate problem is the following: find $\widehat{\boldsymbol{u}} \in L^2(0, T, \widehat{\mathbf{V}}_f) \cap L^\infty(0, T, \mathbf{L}^2(\Omega))$

[5] This denomination is effective but also a little bit misleading, since in any case these conditions "*do something*". This is the reason why we do not adopt this name here.

and $p \in L^2(0,T,Q_f)$ such that for all $\mathbf{v} \in \widehat{\mathbf{V}}_f$ and $q \in Q_f$:

$$\left(\frac{\partial \widehat{\boldsymbol{u}}}{\partial t}, \mathbf{v}\right) + a(\boldsymbol{u}, \mathbf{v}) + c\left(\widehat{\boldsymbol{u}}, \widehat{\boldsymbol{u}}, \mathbf{v}\right) + c\left(\widehat{\boldsymbol{u}}, \sum_{j=1}^{m} Q_j \mathbf{b}_j, \mathbf{v}\right) +$$
$$c\left(\sum_{j=1}^{m} Q_j \mathbf{b}_j, \widehat{\boldsymbol{u}}, \mathbf{v}\right) + b(\mathbf{v}, p) =$$
$$(\mathbf{f}, \mathbf{v}) - \sum_{j=1}^{m} \left(\left(\frac{\partial Q_j}{\partial t}\mathbf{b}_j, \mathbf{v}\right) + Q_j \; a(\mathbf{b}_j, \mathbf{v})\right) - c\left(\sum_{j=1}^{m} Q_j \mathbf{b}_j, \sum_{j=1}^{m} Q_j \mathbf{b}_j, \mathbf{v}\right),$$
$$b(\widehat{\mathbf{u}}, q) = 0, \tag{11.13}$$

with $\widehat{\mathbf{u}}(\boldsymbol{x}, 0) = \boldsymbol{u}_0 - \sum_{j=1}^{m} Q_j(0)\mathbf{b}_j$.

In fact, this formulation forces some conditions implicitly, as stated by the following proposition (for the proof see [218]).

Proposition 11.3.1 *The solution of the flow problems (11.13) fulfills the following boundary conditions on Γ_i, $i = 1, \ldots m$ and for all $t > 0$,*

$$p\boldsymbol{n} - \mu \boldsymbol{\nabla u} \cdot \boldsymbol{n} = C_i \boldsymbol{n}, \quad i = 1, \ldots, m,$$

where $C_i = C_i(t)$ are unknown functions of time.

Remark 11.3.1 *In the case of a problem with flow conditions also on Γ_0, with the constraint on the data $\sum_{i=0}^{m} Q_i = 0$, the previous proposition still holds with $C_0 = C_0(t)$ an arbitrary function of time. The case considered in (11.12) is therefore a special case where we choose $C_0 = 0$. Problem associated to conditions (11.12) is of the same type of the one with all flow boundary conditions and it does not require to force the flow rate compatibility explicitly.*

Concerning the well posedness, we have the following result, proved in [218].

Proposition 11.3.2 *Under suitable assumptions on the smoothness of the domain and the initial data, there exists a time interval in which the flow problem (11.13) is well posed. If $||\boldsymbol{\nabla u}_0||$ and $|Q_i|$ for all i are sufficiently small the solution exists for each $t > 0$.*

This approach has *a practical drawback*. The functional space $\widehat{\mathbf{V}}_f$ is not standard. In view of the numerical approximation, the construction of finite dimensional functional subspaces of $\widehat{\mathbf{V}}_f$, as well as that of the flux carriers is rather problematic.

Different strategies have been proposed that do not suffer from these limitations even if they present other drawbacks.

Augmented formulation

A second approach, proposed in [156], considers the flux conditions as constraints for the solution, to be forced by means of Lagrange multipliers (in a way similar to the treatment of the incompressibility constraint in the mixed formulation of the Navier-Stokes). In practise, we introduce a vector function $\boldsymbol{\lambda}(t)$ and resort to the following problem: find $\mathbf{u} \in L^2(0,T,\boldsymbol{V}_f) \cap L^\infty(0,T,\mathbf{L}^2(\Omega))$, $p \in L^2(0,T,Q_f)$ and $\boldsymbol{\lambda} \in (L^2(0,T))^m$ such that for all $\mathbf{v} \in \boldsymbol{V}_f$, $q \in Q_f$:

$$\begin{aligned}
&\left(\frac{\partial \boldsymbol{u}}{\partial t}, \mathbf{v}\right) + a(\mathbf{u},\mathbf{v}) + c\,(\boldsymbol{u},\boldsymbol{u},\mathbf{v}) + b(\mathbf{v},p) + \sum_{i=1}^{m} \lambda_i \int_{\Gamma_i} \mathbf{v}\cdot\boldsymbol{n}\, d\gamma = (\mathbf{f},\mathbf{v}),\\
&b(\boldsymbol{u},q) = 0,\\
&\int_{\Gamma_i} \mathbf{u}\cdot\boldsymbol{n}\, d\gamma = Q_i \qquad i = 1,2,\ldots m,
\end{aligned} \tag{11.14}$$

Well posedness of this augmented formulation can be proven by means of classical arguments (see [195]). In particular, moving from the well posedness result of Prop. 11.3.2, it can be shown that an inf-sup condition holds for the augmented problem, leading to the following result (see [526]).

Proposition 11.3.3 *Under the same assumptions of Proposition 11.3.2, the augmented formulation (11.14) is well posed.*

Moreover, the investigation of the boundary conditions forced in the augmented formulation so that the problem has a unique solution highlights the physical significance of the Lagrange multiplier. We have in fact the following Proposition (for the proof see [156]).

Proposition 11.3.4 *The solution of problem (11.14) fulfils the following conditions on the artificial boundaries Γ_i, $i = 1,2,\ldots,m$ and for $t > 0$,*

$$P\boldsymbol{n} - \mu\boldsymbol{\nabla u}\cdot\boldsymbol{n} = \lambda_i \boldsymbol{n}. \tag{11.15}$$

In other words, the Lagrange multipliers λ_i do coincide with the functions C_i and play the role of normal stresses on the artificial boundaries.

The augmented formulation is based on standard functional spaces, whose finite dimensional approximations are readily built (and present in most of the commercial packages). However the indefinite saddle point nature of the associated problem needs a specific analysis. Discretisation of (11.14) leads indeed to an algebraic problem that in general is not practical to solve in a monolithic way, i.e. with the simultaneous computation of $\boldsymbol{u}$, P and λ_i.

On the one hand the resulting linear system is in general ill conditioned, on the other hand problem (11.14) is not standard, since it deals with velocity,

pressure and the Lagrange multipliers at the same time. Therefore, the use of existing software packages is complex, if not impossible, in this setting.

These remarks suggest to split apart the computation of the fluid dynamics quantities $(\boldsymbol{u}/P)$ from that of the λ_i, yielding the so-called *segregated methods*. In this perspective, some numerical methods have been proposed in [156, 526, 528] to this aim. We limit ourselves to consider algebraic splittings of the matrix obtained after discretisation/linearisation of the problem at hand at each time step. This system reads $\mathrm{A}\mathbf{y} = \mathbf{c}$, with

$$\mathrm{A} = \begin{bmatrix} \mathrm{C} & \mathrm{D}^T & \mathrm{L}^T \\ \mathrm{D} & \mathbf{0} & \mathbf{0} \\ \mathrm{L} & \mathbf{0} & \mathbf{0} \end{bmatrix}, \qquad \mathbf{c} = \begin{bmatrix} \mathbf{b} \\ \mathbf{0} \\ \mathbf{q} \end{bmatrix}, \tag{11.16}$$

and represents the discrete counterpart of (11.14). Matrix L corresponds to the discretisation of the boundary integrals on Γ_i, D is the discretisation of the divergence operator and C is the result of the discretisation and linearisation of $\left(\dfrac{\partial \boldsymbol{u}}{\partial t}, \mathbf{v}\right) + a(\mathbf{u}, \mathbf{v}) + c\,(\boldsymbol{u}, \boldsymbol{u}, \mathbf{v})$. Correspondingly, $\mathbf{y} = [\mathbf{U}, \mathbf{P}, \boldsymbol{\Lambda}]^T$, contains the nodal values of the unknowns of velocity, pressure and Lagrange multipliers respectively. Finally $\mathbf{b}$ derives from the discretisation of source terms in the momentum equation, and the entries of vector $\mathbf{q}$ are the prescribed flow rates Q_i. Using the notation

$$\mathcal{C} = \begin{bmatrix} \mathrm{C} & \mathrm{D}^T \\ \mathrm{D} & \mathbf{0} \end{bmatrix}, \quad \mathcal{L} = [\mathrm{L}, \mathbf{0}],$$

matrix A can be rewritten in the form:

$$\mathrm{A} = \begin{bmatrix} \mathcal{C} & \mathcal{L}^T \\ \mathcal{L} & \mathbf{0} \end{bmatrix}.$$

Correspondingly, we set $\mathbf{x}_1 = [\mathbf{U},\ \mathbf{P}]^T$ and $\mathbf{x}_2 = \boldsymbol{\Lambda}$, $\mathbf{f}_1 = [\mathbf{b}, \mathbf{0}]^T$ and $\mathbf{f}_2 = \mathbf{q}$.

A possible way for splitting velocity/pressure and multipliers computations is based on the following classical block LU factorisation:

$$\begin{bmatrix} \mathcal{C} & \mathcal{L}^T \\ \mathcal{L} & \mathbf{0} \end{bmatrix} = \begin{bmatrix} \mathcal{C} & \mathbf{0} \\ \mathcal{L} & -\mathcal{L}\mathcal{C}^{-1}\mathcal{L}^T \end{bmatrix} \begin{bmatrix} I & \mathcal{C}^{-1}\mathcal{L}^T \\ \mathbf{0} & I \end{bmatrix},$$

which yields the following three-step algorithm

$$\begin{aligned} &1)\ \mathcal{C}\widehat{\mathbf{x}}_1 = \mathbf{f}_1, \\ &2)\ \mathcal{L}\mathcal{C}^{-1}\mathcal{L}^T\mathbf{x}_2 = \mathcal{L}\widehat{\mathbf{x}}_1 - \mathbf{f}_2, \\ &3)\ \mathcal{C}\mathbf{x}_1 = \mathbf{f}_1 - \mathcal{L}^T\mathbf{x}_2. \end{aligned}$$

We can observe that:

a) steps (1) and (3) require to solve a system in $\mathcal{C}$, i.e. a standard Navier-Stokes problem (see [526]);

b) step (2) consists of solving a problem governed by the $m \times m$ matrix $\mathcal{L}\mathcal{C}^{-1}\mathcal{L}^T$, being m the number of artificial sections where the flow rate is assigned. This is typically a small number in haemodynamics problems (≤ 5). Therefore, a small number of GMRES iterations is in general enough to reach convergence. However, the explicit computation of this matrix is not convenient, since $\mathcal{C}$ is large and sparse and its inversion is expensive and memory consuming due to the well known phenomenon of fill-in. However, iterative methods can avoid the explicit calculation of the matrix, since they only need the application of the current matrix to a vector. This can be done in the following way ($\mathbf{v}, \mathbf{r}, \mathbf{z}$ and $\mathbf{w}$ are vectors of proper dimensions)

$$\mathbf{r} = \mathcal{L}\mathcal{C}^{-1}\mathcal{L}^T\mathbf{v} \Rightarrow \begin{cases} \mathbf{z} = \mathcal{L}^T\mathbf{v}, \\ \mathbf{w} = \mathcal{C}^{-1}\mathbf{z} \Rightarrow \mathcal{C}\mathbf{w} = \mathbf{z}, \\ \mathbf{r} = \mathcal{L}\mathbf{w}. \end{cases}$$

The second step on the right hand side requires again to solve a standard Navier-Stokes problem;

c) step (3) can be rewritten in the form:

$$\mathbf{x}_1 = \mathcal{C}^{-1}\mathbf{f}_1 - \mathcal{C}^{-1}\mathcal{L}^T\mathbf{x}_2 = \widehat{\mathbf{x}}_1 - \mathbf{w}$$

where vector $\mathbf{w} = \mathcal{C}^{-1}\mathcal{L}^T\mathbf{x}_2$ is a by-product of the last iteration of step (2), so this step requires a simple vector sum.

This approach can still be computationally expensive, because of the numerous Navier-Stokes solves involved. The cost is particularly high for unsteady problems, since the algorithm must be applied at each time step. For this reason, some specific techniques for computing an approximate solution to $A\mathbf{y} = \mathbf{c}$ have been devised, like the one in [527] that guarantees that the error introduced is confined in a small neighbourhood of the sections where flow rate are prescribed. In Fig. 11.14 we present an example of solution in a realistic geometrical model of a carotid bifurcation. The heuristic approach based on the prescription of an inlet velocity parabolic profile and a constant pressure profile at the outlet of the internal carotid (on the left) yields a different solution of the velocity field computed than that obtained with the Lagrange multiplier approach (centre). The solution computed by the inexact approach [527] (on the right) is very similar to the Lagrange multiplier one, yet it requires about half of the computational time.

Control approach

Finally, we address a different approach that is in some sense "dual" to the Lagrange multiplier strategy. While in the Lagrangian approach the flow rate boundary conditions are regarded as constraints to the Navier-Stokes equations in the new approach the latter play the role of *state equations*. They act

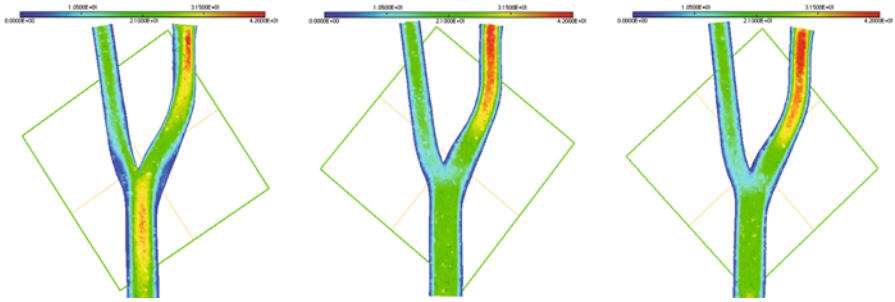

Fig. 11.14. Computations in a 3D carotid bifurcation (the square identifies the cutting plane). Velocity field obtained with the prescription of an inlet parabolic profile (left), the augmented Lagrangian scheme (centre), the inexact approach of [527] (right)

as "constraints" to minimisation of a functional which enforces the desired boundary conditions.

Clearly, for this to work we need to make Navier-Stokes problem function of some parameters, called *control variables*, over which the minimum is sought. The defective boundary problem in this way is formulated as a *control problem* (see e.g. [210]).

For the sake of simplicity, we introduce this approach for the case of the steady Stokes problem. The extension to the unsteady Navier-Stokes problem can be found in [163].

Let us consider the following functional associated with flux conditions (11.12)

$$J_Q : \boldsymbol{V}_f \to \mathbb{R}^+, \quad J_Q(\mathbf{w}) = \frac{1}{2}\sum_{i=1}^{m}\left(\int_{\Gamma_i} \mathbf{w}\cdot\boldsymbol{n}d\gamma - Q_i\right)^2. \tag{11.17}$$

We can formulate the defective boundary problem as follows: minimise $J_Q(\boldsymbol{u}(\mathbf{k}))$ where $\boldsymbol{u}(\mathbf{k})$ is subject to the constraint

$$\begin{aligned}
&-\mu\triangle\boldsymbol{u}(\mathbf{k}) + \nabla P = \mathbf{f}, && \text{in } \Omega\\
&\nabla\cdot\boldsymbol{u}(\mathbf{k}) = 0, && \text{in } \Omega\\
&\boldsymbol{u}(\mathbf{k}) = \mathbf{0}, && \text{on } \Gamma\\
&-P\boldsymbol{n} + \mu\nabla\boldsymbol{u}(\mathbf{k})\cdot\boldsymbol{n} = \mathbf{0}, && \text{on } \Gamma_0\\
&-P\boldsymbol{n} + \mu\nabla\boldsymbol{u}(\mathbf{k})\cdot\boldsymbol{n} = -k_i\boldsymbol{n} && \text{on } \Gamma_i\, i = 1,\ldots,m.
\end{aligned} \tag{11.18}$$

Here, $\mathbf{f} \in \mathbf{L^2(\Omega)}$ is given and the control variables is the vector $\boldsymbol{k}$ whose elements $k_i \in \mathbb{R}$ are the normal components of the stress on the artificial boundaries. In other words, we look for the values of k_i such that the solution of (11.18) minimises J_Q.

To this aim, following e.g. [210], we introduce the constrained functional:

$$\mathcal{L}(\mathbf{w}, s; \boldsymbol{\lambda}_\mathbf{w}, \lambda_s; \boldsymbol{\eta}) = J_Q(\mathbf{w}) + \mu(\nabla \mathbf{w}, \nabla \boldsymbol{\lambda}_w) + b(s, \nabla \cdot \boldsymbol{\lambda}_w) + \sum_{i=1}^{m} \int_{\Gamma_i} \eta_i \boldsymbol{\lambda}_w \cdot \boldsymbol{n} \, d\gamma - (\mathbf{f}, \boldsymbol{\lambda}_w) - (\lambda_s, \nabla \cdot \mathbf{w}).$$

Here $\boldsymbol{\lambda}_\mathbf{w}$ and λ_s are the so-called *adjoint* variables associated with $\mathbf{w}$ and s respectively. Solution is sought by looking for stationary points of $\mathcal{L}$. This turns to be equivalent to solve the following problem[6], where for the sake of brevity we omit to specify that the differentials are computed in $[\mathbf{u}, \mathbf{p}; \boldsymbol{\lambda}_\mathbf{u}, \lambda_\mathbf{p}; \mathbf{k}]$, while we put into evidence the dependence on the control variables.

Given $\mathbf{f} \in \mathbf{L^2}(\boldsymbol{\Omega})$ and $\mathbf{Q} \in \mathbb{R}^\mathbf{m}$, find $\boldsymbol{u}(\mathbf{k}) \in \mathbf{V}, \mathbf{p}(\mathbf{k}) \in \mathbf{L^2}(\boldsymbol{\Omega})$, $\boldsymbol{\lambda}_\boldsymbol{u} \in \mathbf{V}, \lambda_p \in L^2(\Omega)$ and $\mathbf{k} \in \mathbb{R}^m$, such that, for all $\mathbf{v} \in \mathbf{V}$, $q \in L^2(\Omega)$ and $\nu \in \mathbb{R}$:

$$(P) \qquad \langle d\mathcal{L}_{\boldsymbol{\lambda}_\mathbf{w}}, \mathbf{v} \rangle = \mu(\nabla \mathbf{u}, \nabla \mathbf{v}) + b(p, \nabla \cdot \mathbf{v}) + \sum_{i=1}^{m} \int_{\Gamma_i} k_i \mathbf{v} \cdot \mathbf{n} \, d\gamma - (\mathbf{f}, \mathbf{v}) = 0,$$

$$(A) \quad \begin{cases} \langle d\mathcal{L}_\mathbf{u}, \mathbf{v} \rangle = \mu(\nabla \mathbf{v}, \nabla \boldsymbol{\lambda}_\boldsymbol{u}) + b(\lambda_p, \nabla \cdot \mathbf{v}) - \sum_{i=1}^{m} \Big(\int_{\Gamma_i} \boldsymbol{u} \cdot \mathbf{n} \, d\gamma - Q_i \Big) \int_{\Gamma_i} \mathbf{v} \cdot \mathbf{n} \, d\gamma = 0, \\ \langle d\mathcal{L}_s, q \rangle = b(q, \nabla \cdot \boldsymbol{\lambda}_\boldsymbol{u}) = 0, \end{cases}$$

$$(C_j) \quad \langle d\mathcal{L}_{\eta_j}, \nu \rangle = \int_{\Gamma_j} \nu \boldsymbol{\lambda}_\boldsymbol{u} \cdot \mathbf{n} \, d\gamma = 0, \quad j = 1, \ldots, m.$$

Here, $\langle d\mathcal{L}_\mathbf{u}, \mathbf{v} \rangle$ indicates the Gateaux differential with respect to $\boldsymbol{u}$ applied to $\boldsymbol{v}$.

This system couples a steady Stokes problem (P), its adjoint (A) and m scalar equations (*optimality conditions*, denoted by (C_j)). Observe that the last condition forces the adjoint variable $\boldsymbol{\lambda}_\boldsymbol{u}$ to have a null flux on the artificial boundaries. Well posedness of this problem can be proven by resorting to fixed point arguments (see [163]).

The numerical solution of this problem is not a trivial task. A possible approach is to resort to the *steepest descent method* applied to the minimisation of the functional at hand. For more details see [163].

In Fig. 11.15 we report the computation for the same case of Fig. 11.14, solved with the control approach. The differences with the solution computed with the Lagrange multiplier approach, reported in the figure on the right, are below the discretisation errors. The computational cost of this approach

[6] Rigorously speaking, the problem is obtained by forcing the Gateaux differentials of $\mathcal{L}$ evaluated along the direction of any test function to vanish in correspondence of the solution $[\mathbf{u}, \mathbf{p}; \boldsymbol{\lambda}_\mathbf{u}, \lambda_\mathbf{p}; \mathbf{k}]$ (see [210]).

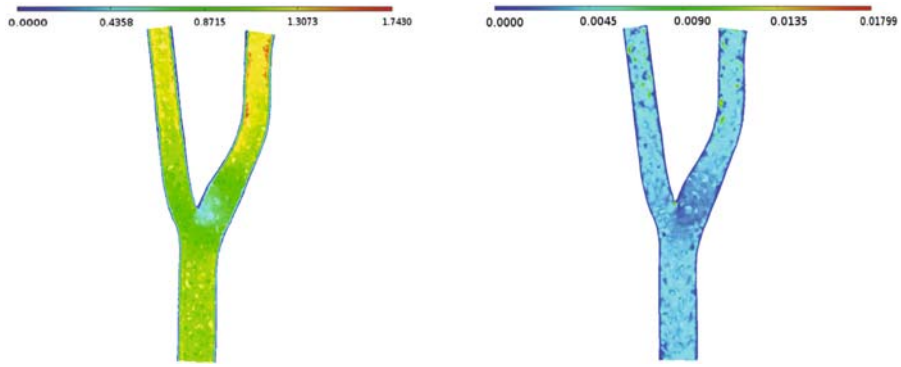

Fig. 11.15. Control approach applied to a flow rate problem in a 3D carotid bifurcation. On the left, the solution obtained by solving the minimisation problem. On the right, plot of the differences with the solution obtained by the Lagrange multiplier approach. The differences are below the discretisation error

can be made comparable with that of the augmented formulation (solved by the splitting scheme) thanks to a proper selection of the iterative solver (see [163]) for the sequence of problems (P), (A) and (C_j). The control approach is however more versatile, as we will illustrate when considering the mean pressure problems.

11.3.2 Mean pressure problem

Let us consider now the following problem: look for $(\boldsymbol{u}, p)$ such that equation (11.9) is satisfied with conditions (11.10) and (11.11) and

$$\int_{\Gamma_i} p d\gamma = P_i, \quad i = 0, 1, \ldots, m, \tag{11.19}$$

where P_i are given functions of time. As for flow rate problem, conditions (11.19) are not enough and some further information need to be prescribed to obtain a well posed problem. Let us illustrate some approaches that aim at completing these conditions in a mathematically sound way.

Again, we will introduce a simple variational approach at first, then we will consider a possible Lagrange multiplier formulation. Both approaches are affected by some important drawbacks that the formulation based on control approach overcomes.

A variational approach

In [218] the following variational formulation of the mean pressure problem is proposed: given $P_i(t)$, $i = 1, 2, \ldots m$, find $(\boldsymbol{u}, P) \in L^2(0, T; \mathbf{H}^1(\Omega)) \times$

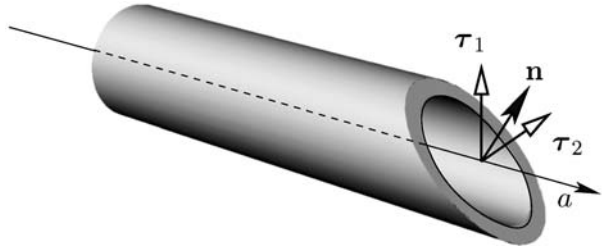

Fig. 11.16. A domain where variational formulation (11.20) for the mean pressure problem is not exact. $\boldsymbol{\tau}_1$ and $\boldsymbol{\tau}_2$ are the directions orthogonal to the axis a and $\mathbf{n}$ is the unit vector orthogonal to the artificial boundary

$L^2(0,T;L^2(\Omega))$ such that for all $\mathbf{v} \in \mathbf{H}^1(\Omega)$ and $q \in L^2(\Omega)$

$$\left(\frac{\partial \boldsymbol{u}}{\partial t}, \mathbf{v}\right) + a(\boldsymbol{u}, \mathbf{v}) + c\,(\boldsymbol{u}, \boldsymbol{u}, \mathbf{v}) + b(\mathbf{v}, p) = (\mathbf{f}, \mathbf{v}) - \sum_{j=1}^{m} P_j \int_{\Gamma_j} \mathbf{v} \cdot \mathbf{n} d\gamma,$$
$$b(\mathbf{u}, q) = 0, \tag{11.20}$$

with $\boldsymbol{u}(\boldsymbol{x}, 0) = \boldsymbol{u}_0(\boldsymbol{x})$.

The boundary conditions added implicitly by this formulation are identified in the following Proposition (see [218]).

Proposition 11.3.5 *Any smooth solution of (11.20) fulfils the following boundary conditions on the artificial boundaries Γ_i, $i = 0, 1, 2, \ldots m$ and for $t > 0$*

$$P\mathbf{n} - \nu \nabla \mathbf{u} \cdot \mathbf{n} = P_i \mathbf{n}. \tag{11.21}$$

In practise, formulation (11.20) forces the mean pressure data by imposing it as a constant normal stress on the artificial boundaries. This is indeed the expected solution in special domains, like a cylindrical rectilinear pipe where Γ_i is normal to the axis. Here, the analytical solution of the mean pressure problem may be computed and satisfies (11.21).

For a generic domain, however, this technique may force a too strong condition, which does not correspond to what is physically expected. This is for instance the case of a rectilinear cylindrical domain with Γ_i oblique to its axis (see Fig. 11.16). Here, we would like the mean pressure problem to reproduce the Poiseulle flow (in steady situations) or the Womersley solution (in a pulsatile flow), which however in this case do not satisfy (11.21). We should therefore consider different approaches.

Augmented formulation

An augmented formulation for pressure drop problems still stems from regarding mean pressure data as constraints for the Navier-Stokes solution, leading

to the problem: find $\mathbf{u} \in L^2(0,T,\boldsymbol{V}_f) \cap L^\infty(0,T,\mathbf{L}^2(\Omega))$, $p \in L^2(0,T,Q_f)$ and $\boldsymbol{\lambda} \in (L^2(0,T))^m$ such that for all $\mathbf{v} \in \boldsymbol{V}_f$, $q \in Q_f$:

$$\begin{aligned}
&\left(\frac{\partial \boldsymbol{u}}{\partial t}, \mathbf{v}\right) + a(\mathbf{u},\mathbf{v}) + c\,(\boldsymbol{u},\boldsymbol{u},\mathbf{v}) + b(\mathbf{v},p) + \sum_{i=1}^{m} \frac{1}{\Gamma_i}\int_{\Gamma_i} P d\gamma = (\mathbf{f},\mathbf{v}),\\
&b(\boldsymbol{u},q) + \sum_{j=0}^{m} \lambda_j \int_{\Gamma_j} q d\gamma = 0, \qquad (11.22)\\
&\frac{1}{|\Gamma_i|}\int_{\Gamma_i} P d\gamma = P_i \qquad i = 1,2,\ldots m.
\end{aligned}$$

Unfortunately, this problem is not well posed. Indeed, it is possible to verify (see [155]) that the conditions forced implicitly by this formulation are

$$\boldsymbol{u}(\mathbf{x},t)\cdot\mathbf{n} = \lambda_i(t) \qquad \text{on} \quad \Gamma_i.$$

In general, since λ_i are non zero constants in space, the latter conditions are incompatible with the fact that $\boldsymbol{u} = \mathbf{0}$ on Γ_w. The discontinuity on $\overline{\Gamma}_i \cap \overline{\Gamma}_w$ leads to a value of the velocity on the boundary which cannot represent a trace for $\mathbf{H}^1(\Omega)$, the natural functional space where we seek the velocity solution of our flow problem. Indeed, the augmented formulation is appropriate in the case where only a slip condition (i.e $\boldsymbol{u}\cdot\boldsymbol{n} = 0$) is imposed on Γ_w, a situation which however is not physical for a Navier-Stokes problem.

For this reason, the augmented formulation for mean pressure drop problems is not investigated any further.

Control approach

The approach based on control theory presented for the flow rate problems can be straightforwardly extended to the mean pressure problem. With this aim, we introduce the following functional

$$J_P(s) = \frac{1}{2}\Big(\sum_{i=0}^{m} \frac{1}{|\Gamma_i|}\int_{\Gamma_i} s\, d\gamma - P_i\Big)^2 \qquad (11.23)$$

and, as for the flow rate conditions, we consider a constrained minimisation problem. Again, we assume that Navier-Stokes equations play the role of constraint for the solution minimising (11.23). As control variables we still assume the constant normal stresses $\mathbf{k} = [k_i]$. It is worth remarking that this is not the only possibility, since other choices for the control variables can be pursued, such as flow rates (see [163]).

Still referring to steady Stokes equations for the sake of simplicity, we introduce the following Lagrange functional:

$$\begin{aligned}
\mathcal{L}(\mathbf{w},s;\boldsymbol{\lambda}_w,\lambda_s;\boldsymbol{\eta}) = J_P(s) + a(\mathbf{w},\boldsymbol{\lambda}_w) + d(s,\boldsymbol{\lambda}_w)\\
+ \sum_{i=0}^{m}\int_{\Gamma_i} \eta_i\boldsymbol{\lambda}_w\cdot\mathbf{n}\, d\gamma - (\mathbf{f},\boldsymbol{\lambda}_w) + d(\lambda_s,\mathbf{w}).
\end{aligned}$$

A stationary point of $\mathcal{L}$ satisfies the following problem: given $\mathbf{f} \in \mathbf{L}^2(\Omega)$ and $P_j \in \mathbb{R}$, $j = 0, \ldots, m$, find $\mathbf{k} \in \mathbb{R}^m$, $\mathbf{u}(\mathbf{k}) \in \mathbf{V}_{div}, p(\mathbf{k}) \in H^1(\Omega), \boldsymbol{\lambda}_u \in \mathbf{V}_{div}$ and $\lambda_p \in H^1(\Omega)$, such that, for all $\mathbf{v} \in \mathbf{V}_{div}$, $q \in H^1(\Omega)$ and $\nu \in \mathbb{R}$,

$$(P) \begin{cases} \langle d\mathcal{L}_{\boldsymbol{\lambda}_u}, \mathbf{v} \rangle = a(\mathbf{u}, \mathbf{v}) + d(p, \mathbf{v}) + \displaystyle\sum_{i=0}^{m} \int_{\Gamma_i} k_i \mathbf{v} \cdot \mathbf{n} \, \mathbf{d}\gamma - (\mathbf{f}, \mathbf{v}) = \mathbf{0}, \\ \langle d\mathcal{L}_{\lambda_p}, q \rangle = d(q, \mathbf{u}) = \mathbf{0}, \end{cases}$$

$$(A) \begin{cases} \langle d\mathcal{L}_{\mathbf{u}}, \mathbf{v} \rangle = a(\mathbf{v}, \boldsymbol{\lambda}_{\boldsymbol{u}}) + d(\lambda_p, \mathbf{v}) = 0, \\ \langle d\mathcal{L}_p, q \rangle = \displaystyle\sum_{i=0}^{m} \Big(\frac{1}{|\Gamma_i|} \int_{\Gamma_i} p \, d\gamma - P_i \Big) \frac{1}{|\Gamma_i|} \int_{\Gamma_i} q \, d\gamma + d(q, \lambda_{\mathbf{u}}) = \mathbf{0}, \end{cases}$$

$$(C_j) \quad \langle d\mathcal{L}_{k_i}, \nu \rangle = \int_{\Gamma_i} \nu \lambda_{\mathbf{u}} \cdot \mathbf{n} \, \mathbf{d}\gamma = \mathbf{0}, \quad \mathbf{i} = \mathbf{0}, \ldots, \mathbf{m}.$$

One of the most interesting features of this approach is that functional to be minimised can be adjusted for including some possible a priori information on the behaviour of the solution on artificial boundaries. For instance, for a boundary of a pipe non orthogonal to the axis (see Fig. 11.16), where formulation (11.20) fails, the functional to be minimised can be adapted in order to include the physical evidence of the prevalent axial direction of the flow. We resort in this case to the functional

$$\mathcal{L}(\mathbf{w}, s; \boldsymbol{\lambda}_w, \lambda_s; \boldsymbol{\eta}) = J_P(s) + a(\mathbf{w}, \boldsymbol{\lambda}_w) + d(s, \boldsymbol{\lambda}_w) + \sum_{i=0}^{m} \int_{\Gamma_i} \eta_i \boldsymbol{\lambda}_w \cdot \mathbf{n} \, d\gamma - (\mathbf{f}, \boldsymbol{\lambda}_w) + d(\lambda_s, \mathbf{w}) + \mathcal{S}(\mathbf{w}, \boldsymbol{\tau}_1, \ldots, \boldsymbol{\tau}_m) \quad (11.24)$$

where in a problem with d space dimensions

$$\mathcal{S}(\mathbf{w}, \boldsymbol{\tau}_1, \ldots, \boldsymbol{\tau}_m) = \frac{1}{2} \sum_{l=1}^{d-1} \sum_{i=0}^{m} \int_{\Gamma_i} |\mathbf{w} \cdot \boldsymbol{\tau}_l|^2 \, d\gamma, \quad (11.25)$$

and τ_l are the orthogonal directions to the pipe axis a, which in this case do not coincide with the tangential directions to the boundary Γ_i. The term $\mathcal{S}$ forces the velocity components orthogonal to a to be small. With a proper choice of control variables, this procedure yields good numerical results.

For instance, suppose to prescribe a mean pressure $\int_\Gamma p d\gamma = P = 1\,\mathrm{g}/(\mathrm{s}^2\,\mathrm{cm})$ at the outlet Γ_{out} of the domain T (see Fig. 11.17 top). Boundary Γ_{out} is supposed to be an artificial boundary in a pipe where a Poiseuille flow holds, so that vertical velocity is zero.

By minimising functional (11.23), an undesirable vertical velocity at the outlet occurs (Fig. 11.17, centre) while this is not anymore the case when using the penalised functional (11.24) with (11.25) and the complete stress (normal and tangential) as control variables. Fig. 11.17, bottom, show that the latter strategy is able to strongly reduce the wrong tangential velocities.

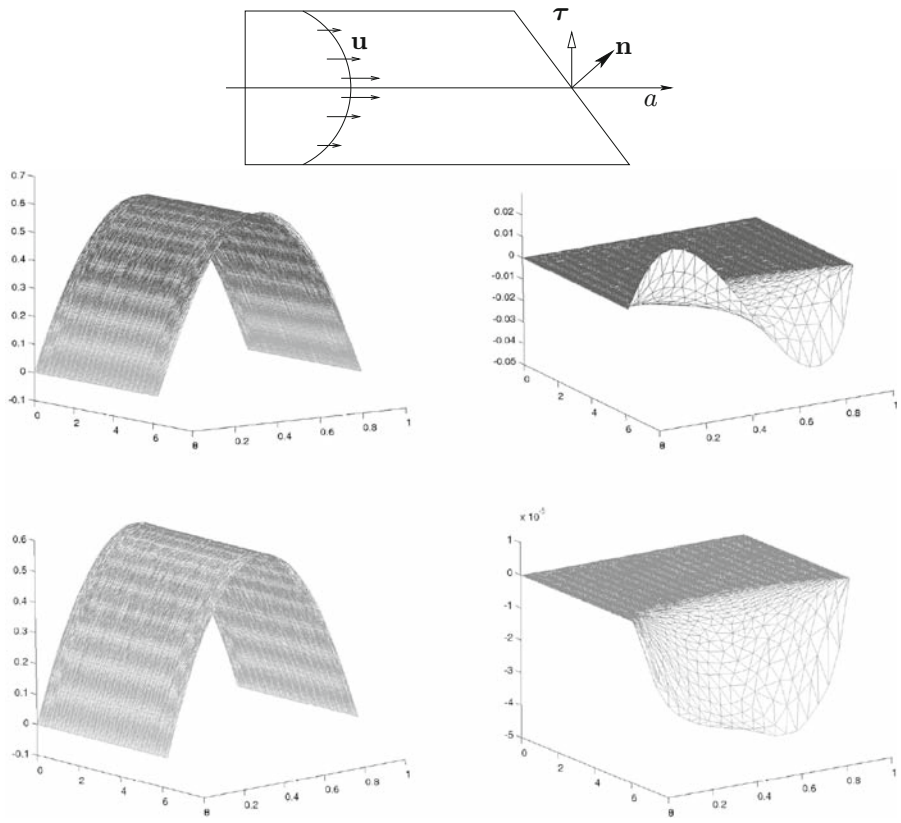

Fig. 11.17. Simulations in a 2D pipe with an oblique boundary: in the centre axial and normal velocity components by solving a mean pressure problem with the minimisation of (11.23). On the bottom the same problem solved by minimising (11.25): the velocity component along $\boldsymbol{\tau}$ is strongly reduced (maximum value in the last figure is 10^{-5})

Remark 11.3.2 *As previously pointed out, different variational formulations lead to different boundary conditions. For instance, if we exploit the vector identity* $\nabla(1/2|\mathbf{u}|^2) = \mathbf{u} \cdot (\nabla \mathbf{u})^T$*, momentum equations can be equivalently reformulated*

$$\frac{\partial \boldsymbol{u}}{\partial t} + \boldsymbol{u} \cdot \nabla \boldsymbol{u} - \boldsymbol{u} \cdot (\nabla \mathbf{u})^T - \nu \triangle \boldsymbol{u} = -\nabla \left(P + \frac{1}{2}|\boldsymbol{u}|^2 \right).$$

Variational formulations associated to this form lead to natural conditions where the total pressure $P + \frac{1}{2}|\boldsymbol{u}|^2$ *replaces the pressure* P*. This form of the momentum equations is therefore well suited for defective boundary conditions on the total pressure. Other strong formulations of the momentum equations well suited for other kinds of boundary conditions are considered in [32].*

11.3.3 Defective boundary problems: the compliant case

When describing a compliant domain, different models for the vessel mechanics could be considered, as discussed in Chapter 3. Models which do not involve a differential operator for the space variables, like the algebraic laws considered in Chapter 10 do not need boundary conditions for the wall problem. Models which exhibit second order differential operators in space, on the contrary, require boundary conditions on the artificial boundaries that typically either prescribe the position $\mathbf{d}$ or the normal stresses (see Chapter 3). In this case, defective problems occur also for the structure problem and a complete analysis is still missing. Here, we limit ourselves to some basic remarks.

Possible approaches are suggested by the strategies presented in the rigid case. For instance, let us assume that a boundary condition is prescribed on the *area* of the $i-$th artificial section

$$\int_{\Gamma_i(\mathbf{d})} d\gamma = A_i(t). \tag{11.26}$$

This condition can come from coupling a 3D compliant model with a 1D model or can be inferred by measurements. It is clear that (11.26) can be regarded in general as an *average* condition for the vascular wall position. As a matter of fact, assume that the interface Γ_i is planar and the z-axis is aligned along its normal. Then, we may write

$$\boldsymbol{d}(x, y, z, t) = \begin{cases} \sqrt{x^2(t) + y(t)^2} = R_i(\theta, t), \\ z = z_i, \end{cases}$$

where $\theta = \tan^{-1}(y/x)$. In this case, condition (11.26) provides

$$\int_0^{2\pi} \int_0^{R(\theta,t)} \rho d\rho d\theta = A_i(t). \tag{11.27}$$

As done in Section 11.2 (eq. (11.4)), we can pursue a heuristic approach similar to the one for flow rates. The latter was essentially based on the a-priori selection of a velocity profile, so that condition (11.27) can be fulfilled by arbitrarily selecting a profile for $R_i(\theta, t)$. In particular, assumption of a circular shape implies to take R_i independent of θ. In this way, (11.27) reduces to

$$\pi R_i^2(t) = A_i(t) \Rightarrow R_i(t) = \sqrt{\frac{A_i(t)}{\pi}}.$$

More in general, one can set $R_i(t, \theta) = C_i(t) R_0(\theta)$ where $C_i(t)$ is selected in such a way that:

$$C_i^2(t) \int_0^{2\pi} \frac{R_0^2(\theta)}{2} d\theta = A_i(t).$$

In practise, this amounts to assume that boundary area evolves according to a homothety of the reference area described by $R_0(\theta)$ (see [52]).

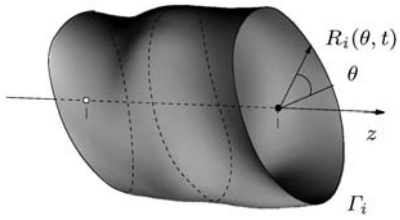

Fig. 11.18. "Artificial" section of a compliant domain

As for the case of flow rate conditions, this strategy upgrades defective data for the displacement to classical Dirichlet conditions and actually requires low computational costs. This is an important feature in particular for fluid-structure interaction problems which are usually computationally very expensive.

However, different mathematically sound approaches can still be pursued. Control approach can be extended to the compliant case, by including conditions on structure in the functional to be minimised. For instance, pressure and area conditions in the form

$$\int_{\Gamma_i} P da = P_i, \qquad \int_{\mathbf{x}\in\Gamma_i(\boldsymbol{d})} d\gamma = A_i \tag{11.28}$$

can be faced by resorting to the minimisation of

$$\mathcal{J}_{p,A} = \frac{1}{2}\left(\int_{\Gamma_i} P da - P_i\right)^2 + \left(\int_{\mathbf{x}\in\Gamma_i(\boldsymbol{d})} d\gamma - A_i\right)^2$$

with the constraint given by fluid-structure equations.

Another possible approach refers to the augmented formulation. In [352] an augmented formulation for a compliant 3D model is considered with flow rate boundary conditions. Since no data were available for the structure, homogeneous natural conditions have been introduced. In Fig. 11.19 we report the

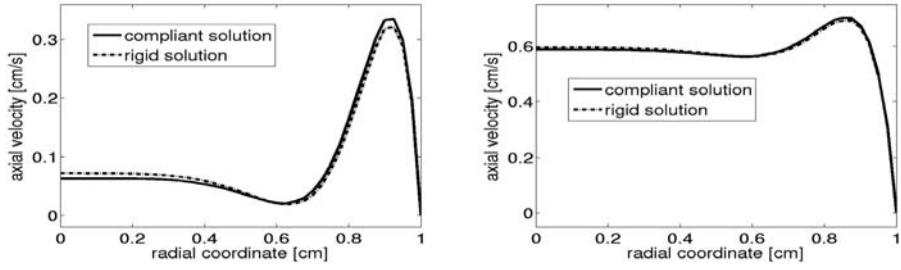

Fig. 11.19. Comparison between the inlet profiles in a rigid and compliant simulation. The results are obtained by prescribing the sinusoidal in time flow rates with a Lagrange multiplier approach [352]

velocity profile computed with this approach at the inlet of a compliant vessel, compared to the solution of the corresponding rigid case. The solution is axial-symmetric, so that only half profile is reported.

11.4 Some well posedness results

In this section we recall some theoretical results on multiscale models. We illustrate in particular some stability properties concerning the coupling of 3D and 1D models. Then we will present a general well posedness analysis of 3D/0D models and its extension to the 1D/0D case.

11.4.1 Coupling of 3D and 1D models

Referring to Fig. 11.20, let us consider a $3D-1D$ coupling, where for the sake of simplicity we assume that the interface between the models is normal to the z axis. The $3D$ model is given by

$$\begin{aligned}
&\frac{\partial \boldsymbol{u}}{\partial t} + \left(\frac{1}{2}\nabla|\boldsymbol{u}|^2 + (\nabla \times \boldsymbol{u}) \times \boldsymbol{u}\right) - \nabla \cdot (2\nu \mathbf{D}(\boldsymbol{u})) + \nabla P = \mathbf{f} \quad \mathbf{x} \in \Omega_f, t > 0,\\
&\nabla \cdot \boldsymbol{u} = 0 \qquad \mathbf{x} \in \Omega_f, t > 0,\\
&\rho_w \frac{\partial^2 \eta_r}{\partial t^2} + \sigma \eta_r = \Phi_r - \Phi_{ext} \quad \mathbf{x} \in \Gamma_w, t > 0,
\end{aligned} \tag{11.29}$$

where ρ_w is the wall density, η_r is the radial displacement, while we assume that axial and circumferential displacements are null, and $\Phi_r - \Phi_{ext}$ is the difference of stresses in the radial direction induced by the fluid and the external organs. Observe that the structure is modelled by the *independent rings model* (structure is considered as a stack of independent slices or rings), while the convective term of the fluid problem has been rearranged in order to have natural conditions associated with the total pressure (see Remark 11.3.2). System is completed by the initial conditions $\eta_r(\mathbf{x}, 0) = \eta_0$, $\dfrac{\partial \eta_r}{\partial t}(\mathbf{x}, 0) = u_r$ for $\mathbf{x} \in \Gamma_w$

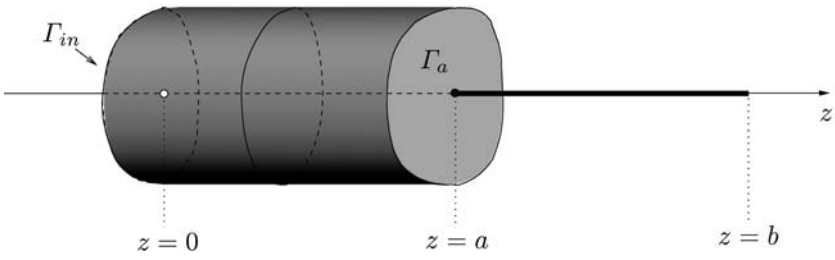

Fig. 11.20. Domain for the coupled 3D/1D problem

and $\boldsymbol{u}(\mathbf{x},0)=\boldsymbol{u}_0$ for $\mathbf{x}\in\Omega$. At the inlet Γ_{in} of the 3D domain we can assume both Dirichlet and Neumann conditions for the Navier-Stokes equations.

For $z\in(a,b)$ we assume the 1D model to satisfy equations (10.27) that we report here for completeness

$$\begin{aligned}&\frac{\partial A}{\partial t}+\frac{\partial Q}{\partial x}=0,\\&\frac{\partial Q}{\partial t}+\frac{\partial}{\partial x}\left(\alpha\frac{Q^2}{A}\right)+\frac{A}{\rho}\left(\frac{\partial p}{\partial x}\right)+K_R\frac{Q}{A}=0.\end{aligned}$$

We assume also that area and pressure are related by the algebraic law (see Section 10.1.1)

$$P-P_{ext}=\psi(A,A_0,\beta)=\beta\frac{\sqrt{A}-\sqrt{A_0}}{A_0}.$$

On $z=b$ we assume absorbing boundary conditions, while in $z=a$ we set

$$\begin{aligned}&\left(\left(P+\frac{1}{2}|\boldsymbol{u}|^2\right)\mathbf{I}-2\nu\mathbf{D}(\boldsymbol{u})\right)\cdot\boldsymbol{n}=P_{1D}+\frac{1}{2}|\overline{u}_{1D}|^2,\\&\int_{\Gamma_f}\boldsymbol{u}\cdot\boldsymbol{n}d\gamma=Q_{1D}.\end{aligned}\tag{11.30}$$

To the 3D model we associate the following energy functional

$$\mathcal{E}_{3D}=\frac{1}{2}||\boldsymbol{u}||^2_{L^2(\Omega_f(t))}+\frac{\rho_w}{2}||\frac{\partial\eta_r}{\partial t}||^2_{L^2(\Gamma_{w,0})}+\frac{b}{2}||\eta_r||^2_{L^2(\Gamma_{w,0})}$$

where $\Omega_f(t)$ is the fluid domain at time t while $\Gamma_{w,0}$ is the reference structure domain, which here reduces to the wall boundary of $\Omega_f(0)$. For the 1D model, we select the following energy

$$\mathcal{E}_{1D}=\frac{1}{2}\int_a^b\frac{Q^2}{A}dz+\int_a^b\int_{A_0}^A\psi(\tau,A_0,\beta)d\tau dz.$$

We have then (see [159]) the following Proposition.

Proposition 11.4.1

1. *If homogeneous Dirichlet conditions for the velocity are prescribed on Γ_{in}, the following (*energy decay property*) holds*

$$\mathcal{E}_{3D}(t)+\nu\int_0^t||\mathbf{D}(\boldsymbol{u})||^2_{L^2}dt+\mathcal{E}_{1D}(t)K_r\int_0^t\int_a^b\frac{Q^2}{A^2}dzdt\le\mathcal{E}_{3D}(0)+\mathcal{E}_{1D}(0).$$

2. If non homogeneous Neumann conditions for the fluid are prescribed on Γ_{in} with data $\mathbf{g}$*, we have (*energy estimate*)*

$$\mathcal{E}_{3D}(t) + \nu \int_0^t ||\mathbf{D}(\boldsymbol{u})||^2_{L^2} dt + \mathcal{E}_{1D}(t) K_r \int_0^t \int_a^b \frac{Q^2}{A^2} dz dt \leq$$
$$\left(\mathcal{E}_{3D}(0) + \mathcal{E}_{1D}(0) + C \int_0^t ||\mathbf{g}||^2_{L^2(\Gamma_i n)}\right) e^{2\nu t}.$$

Remark 11.4.1 *The previous results can be extended to more complex domains with many interfaces between 3D and 1D models. As a matter of fact, they can be applied locally at each interface.*

11.4.2 Coupling of 3D and 0D models

We consider now the multiscale 3D/0D depicted in Fig. 11.18. In particular we make the following basic assumptions.

1. The NS model is given in terms of classical primitive variable formulation of Navier-Stokes equations. We assume that initial data and forcing terms are small enough, for the sake of well-posedness of the problem (see [218]).
2. Nonlinear terms of K model (introduced by the modelling of valves and of the heart action) are described by suitable smooth functions (see Chapter 10).

This coupled problem can be analysed by a fixed point strategy represented in Fig. 11.21. Precisely, we regard the solution as the fixed point of an operator $\mathcal{T}$ given by the sequence of NS and K problems (denoted respectively as $\mathcal{P}_{NS}$ and $\mathcal{P}_K$). Setting $\mathcal{T} = \mathcal{P}_K \cdot \mathcal{P}_{NS}$ the solution to the coupled multiscale problem satisfies

$$\overline{\mathbf{s}} = \mathcal{T}\overline{\mathbf{s}} = \mathcal{P}_K \cdot \mathcal{P}_{NS}\overline{\mathbf{s}}.$$

In this framework, we add two further assumptions.

3. The splitting into subproblems $\mathcal{P}_{NS}$ and $\mathcal{P}_K$ represented in Fig. 11.21 is bridging region compatible. With reference to Fig. 11.18, the role of interface variables in the splitting is given in Table 11.1.
4. Defective boundary problem $\mathcal{P}_{NS}$ is formulated in terms of variational formulations following the variational approach advocated in Section 11.3.

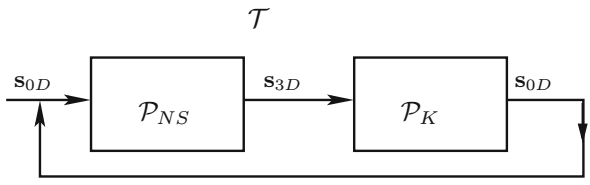

Fig. 11.21. Splitting/fixed point reformulation of multiscale model of Fig. 11.18

Table 11.1. Role of matching data in a bridging region compatible splitting for multiscale model depicted in Fig. 11.12

	Input $\mathcal{P}_{NS}$ = *Output* $\mathcal{P}_K$	*Input* $\mathcal{P}_K$ = *Output* $\mathcal{P}_{NS}$
Γ_0	pressure P_0	flow rate Q_0
Γ_1	flow rate Q_1	pressure P_1
Γ_2	flow rate Q_2	pressure P_2

More precisely, let $\widehat{\mathbf{V}}_f$ denote the space

$$\widehat{\mathbf{V}}_f \equiv \left\{ \mathbf{v} \in \boldsymbol{V}_f : \int_{\Gamma_0} \mathbf{v} \cdot \boldsymbol{n} = 0 \right\},$$

and $\mathbf{b}_0$ a function of $\boldsymbol{V}_f$ such that $\displaystyle\int_{\Gamma_0} \mathbf{b}_0 \cdot \boldsymbol{n}\, d\gamma = 1$. Set $\boldsymbol{u} = \widehat{\boldsymbol{u}} + Q_0 \mathbf{b}_0$. The following variational formulation holds. Find $\widehat{\boldsymbol{u}} \in L^2(0,T,\widehat{\mathbf{V}}_f) \cap L^\infty(0,T,\mathbf{L}^2(\Omega))$ and $p \in L^2(0,T,Q_f)$ such that for all $\mathbf{v} \in \widehat{\mathbf{V}}_f$ and $q \in Q_f$:

$$\begin{aligned}
&\left(\frac{\partial \widehat{\boldsymbol{u}}}{\partial t}, \mathbf{v}\right) + a(\boldsymbol{u}, \mathbf{v}) + c\left(\widehat{\boldsymbol{u}}, \widehat{\boldsymbol{u}}, \mathbf{v}\right) + c\left(\widehat{\boldsymbol{u}}, Q_0\mathbf{b}_0, \mathbf{v}\right) + c\left(Q_0\mathbf{b}_0, \widehat{\boldsymbol{u}}, \mathbf{v}\right) + \\
&b(\mathbf{v}, p) = (\mathbf{f}, \mathbf{v}) - \left(\frac{\partial Q_0}{\partial t}\mathbf{b}_0, \mathbf{v}\right) + Q_0\ a(\mathbf{b}_0, \mathbf{v}) - c\left(Q_0\mathbf{b}_0, Q_0\mathbf{b}_0, \mathbf{v}\right) - \\
&P_1 \int_{\Gamma_1} \mathbf{v} \cdot \boldsymbol{n}\, d\gamma - P_2 \int_{\Gamma_2} \mathbf{v} \cdot \boldsymbol{n}\, d\gamma, \\
&b(\widehat{\mathbf{u}}, q) = 0,
\end{aligned} \tag{11.31}$$

with $\widehat{\mathbf{u}}(\boldsymbol{x}, 0) = \boldsymbol{u}_0 - Q_0(0)\mathbf{b}_0$.

By collecting classical results of calculus and results proven in [218], [121], we have that:

1. **NS Problem:** If initial and forcing data are small enough, $\mathcal{P}_{NS}$ is well posed.
2. **K Problem:** DAE system of $\mathcal{P}_K$ is of index 1 and can be reformulated as a well posed Cauchy problem.
3. **Multiscale:** There exists $T^\star > 0$ such that $\mathcal{T}$ is *compact* in $(0, T^\star]$. This means that the application of $\mathcal{T}$ to bounded sequences of arguments yields *convergent* sequences in appropriate topologies (for a more precise definition of compactness see e.g. [556]).

The latter step actually proves the existence of a fixed point, thanks to the classical *Schauder's fixed point theorem* (see [409]).

11.4.3 Coupling of 1D and 0D models

Following a similar outline as for the 3D-0D coupling, in [147] the coupling between 1D and 0D models is investigated. It is assumed that the 1D model is

represented in terms of characteristic variables $\mathbf{W}$ and that the DAE system of lumped parameters model is reduced to an ordinary differential system, so that the coupled model reads

$$\begin{aligned} &\frac{\partial \mathbf{W}}{\partial t} + \begin{bmatrix} \mu(W_1, W_2) & 0 \\ 0 & \lambda(W_1, W_2) \end{bmatrix} \frac{\partial \mathbf{W}}{\partial x} = 0, \qquad \text{in} \quad \mathbb{R}^+ \times [0, T], \\ &\frac{d\mathbf{y}}{dt} = \mathcal{G}(\mathbf{y}, t) + \mathbf{f} \qquad \text{in} \quad [0, T]. \end{aligned} \tag{11.32}$$

System (11.32) is completed by initial conditions $\mathbf{w}(x, 0) = \mathbf{w}_0(x)$, $\mathbf{y}(x, 0) = \mathbf{y}_0(x)$ and the matching conditions:

$$W_1(a, t) = g(\mathbf{y}, W_2), \mathbf{f} = \mathbf{f}(\mathbf{W}),$$

where $x = a$ is the interface between the two submodels, g is a suitable function relating the characteristic variable W_1 with the entry of the state vector $\mathbf{y}$ associated with the interface condition, for instance the interface pressure, and correspondingly forcing term $\mathbf{f}$ would depend on the interface flow rate $Q = Q(\mathbf{W})$.

Results obtained for the 3D/0D coupling can be strengthened in the case of 1D/0D problems. In fact the analysis can be carried out again by reformulating this problem in a fixed point framework. Let $\mathcal{P}_K$ be the operator corresponding to solve the lumped parameter model for a given flow rate Q at the interfaces and $\mathcal{P}_E$ be the operator corresponding to solve 1D model for given pressure interfaces and to compute the associated interface flow rates. Then the problem at hand can be reformulated as the search of the fixed point for the operator:

$$\mathcal{T} = \mathcal{P}_E \cdot \mathcal{P}_K.$$

Under mild assumptions on the regularity of the initial data and on λ and μ it is possible to prove that:

1. $\mathcal{P}_K$ is well posed for $0 < t \leq T_0$ with $T_0 \leq T$;
2. $\mathcal{P}_E$ is well posed for $0 < t \leq T_1$ with $T_1 \leq T$;
3. $\mathcal{T}$ is a *contraction* in $0 < t \leq \hat{T} \leq \min(T_0, T_1)$, i.e.

$$||\mathcal{T}(Q_1) - \mathcal{T}(Q_2)||_{C^0[0,\hat{T}]} \leq K||u_1 - u_2||_{C^0[0,\hat{T}]}$$

with $K < 1$, being Q_1 and Q_2 two interfaces flow rates properly selected.

The latter inequality is stronger than the compactness proved for the corresponding operator in the 3D/0D. In particular, well known *Banach contraction theorem* (see e.g. [556]) proves in this case that the solution to the coupled problem exists and it is unique.

Recent results on the coupled problem stating the existence of local and global classical solutions under assumptions on the data may be found in [435–437].

11.5 Numerical techniques for the coupling

We here consider possible numerical techniques for the coupled problems. In particular we will distinguish between monolithic solvers where the coupled problem is treated as a whole and substructuring-type solvers. In the latter, the solution is sought by an iterative procedure where each model is computed in sequence. Monolithic solvers avoid the problem of setting up a fast convergent sequence of iterates. Yet, they may be more difficult to implement and sometimes give rise to badly conditioned problems. Substructuring procedures, on the other hand, may allow to use existing software already developed for solving subproblems separately.

11.5.1 Monolithic solvers

Let us start by considering the case of a 3D-0D coupled problem where K models describe terminal vessels, as we have done in Section 10.1.5. More precisely, we assume that the presence of terminal vessels is described in the frequency domain by means of an appropriate impedance function $\zeta_i(\omega)$ for $i = 1, 2, \ldots, m$ (see Chapter 10) to be coupled to the 3D problem at the m distal boundaries of the latter. On the proximal boundaries of the NS problem we assume for the sake of simplicity that boundary data (pressure or flow rates) are given, for instance by measurements (see Fig. 11.22, where $m = 2$).

If $\pi_i(\omega)$ and $\chi_i(\omega)$ represent the Fourier transform of the interface pressures $P_i(t)$ and flow rates $Q_i(t)$ respectively, the 0D model would provide a relation in the frequency domain of the type

$$\pi_i(\omega) = \zeta_i(\omega)\chi_i(\omega),$$

which, transformed back to the time domain gives

$$P_i(t) = \frac{1}{T}\int_{t-T}^{t} Z_i(t-\tau)Q_i(\tau)d\tau. \tag{11.33}$$

Here Z_i is the inverse Fourier transform of ζ_i and T is the heart beat period. Conditions (11.33) cannot be regarded as mean pressure boundary conditions,

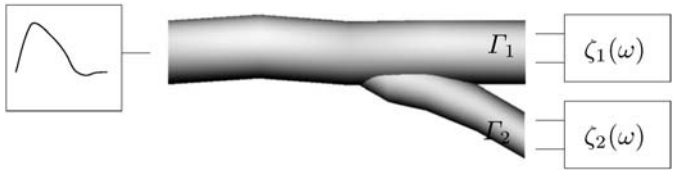

Fig. 11.22. 3D/0D coupling with K models described by impedance functions ζ_1 and ζ_2 in the frequency domain. Here lumped parameters model have the role of describing terminal vessels (see Section 10.1.5)

since the pressure is given as a function of the (unknown) flow rate. However, we can recast (11.33) in the variational formulation of the 3D NS problem in a way similar to the one pursued for the variational formulation of the mean pressure problem (see (11.20)). We set (for $j = 1, \ldots, m$)

$$\int_{\Gamma_j} (P\boldsymbol{n} - \nu \mathbf{D}(\boldsymbol{u}) \cdot \boldsymbol{n}) \cdot \mathbf{v} d\gamma = P_j \int_{\Gamma_j} \boldsymbol{n} \cdot \mathbf{v} d\gamma.$$

In this way, a variational formulation of the 3D/0D coupled problem reads:

$$\begin{aligned} &\left(\frac{\partial \boldsymbol{u}}{\partial t}, \mathbf{v}\right) + a(\boldsymbol{u}, \mathbf{v}) + c(\boldsymbol{u}, \boldsymbol{u}, \mathbf{v}) + b(\mathbf{v}, p) + \sum_{j=1}^{m} T_j^{0D} = (\mathbf{f}, \mathbf{v}), \\ &b(\mathbf{u}, q) = 0, \end{aligned} \tag{11.34}$$

where

$$T_j^{0D} = \frac{1}{T} \int_{t-T}^{t} Z_j(t-\tau) \int_{\Gamma_j} \boldsymbol{u}(\tau) \cdot \mathbf{n} d\tau \int_{\Gamma_j} \mathbf{v} \cdot \mathbf{n} d\gamma. \tag{11.35}$$

In practise, we obtain special Robin boundary conditions for the Navier-Stokes problem.

Discretisation of this problem can be carried out by means of methods addressed in Chapter 2. For instance, if space discretisation is based on the finite element method and time discretisation on finite differences, then velocity field at time t^n is represented as

$$\boldsymbol{u}_h(\boldsymbol{x}, t^n) = \sum_i \mathbf{U}_i^n \boldsymbol{\varphi}_i(\boldsymbol{x})$$

being $\boldsymbol{\varphi}_k$ the Lagrangian basis functions of the finite element space and $\mathbf{U}_k^n$ the nodal values vector. The term on the right hand side of (11.35) can be discretised in time by resorting to classical quadrature formulae. If the quadrature nodes do coincide with time levels, we have simply

$$\begin{aligned} &\frac{1}{T} \int_{t^{n+1}-T}^{t^{n+1}} Z_j(t^{n+1} - \tau) \int_{\Gamma_j} \boldsymbol{u}(\tau) \cdot \mathbf{n} d\tau \int_{\Gamma_j} \mathbf{v} \cdot \mathbf{n} d\gamma \approx \\ &\qquad \frac{1}{T} \left(\sum_{k=\underline{k}}^{\overline{k}} w_k Z_j(t^{n+1} - t^k) \int_{\Gamma_j} \boldsymbol{\varphi}_j \cdot \mathbf{n} \sum_l \int_{\Gamma_j} \boldsymbol{\varphi}_l \cdot \mathbf{n} \right) \mathbf{U}_j^l, \end{aligned}$$

where w_k are the quadrature weights and the quadrature nodes are such that $T - t^{n+1} \leq t^{\underline{k}} \leq t^{\underline{k}+1} \leq \ldots \leq t^{\overline{k}-1} \leq t^{\overline{k}} \leq t^n$.

Remark 11.5.1 *In the oversimplified case of a purely resistive impedance function $Z_j(t) = R_j T \delta(t)$, being δ the Dirac generalised function, and we have*

$$T_j^{0D} = R_j \int_{\Gamma_j} \boldsymbol{u}(t) \cdot \mathbf{n} d\gamma \int_{\Gamma_j} \mathbf{v} \cdot \mathbf{n} d\gamma.$$

This approach has been adopted for instance in [531] where the relevance of an appropriate impedance function is clearly shown by numerical results.

An algebraic formulation

Thus far, we have considered a monolithic formulation of a coupled 3D/0D problem in which however the primal role of K models was to provide boundary conditions which could well represent the general behaviour of the vascular tree external to the 3D model. In particular, blood dynamics in terminal vessels is computed only as far as it influences the 3D solution at the interfaces.

Let us consider now a different approach in which one is interested also to the evolution of the state variables in the lumped parameter model. We assume therefore to describe 0D problems in the time domain as a system of ordinary differential equations.

For the sake of clarity we will consider an example, namely the multiscale problem represented in Fig. 11.23, where the K model is given by a network featuring a capacitance C, three resistances and three inductors. The forcing term in the network is given by a voltage/pressure generator where $P_p(t)$ is a given function. The NS model is given by Navier-Stokes equations and bridging region compatibility requires that flow rate is prescribed at the boundaries of 3D domain. A model for the compliance of the wall can be included as well. For the sake of simplicity however we assume that the pipe is rigid, so that flow rate at inflow must equal that at outflow. Equations associated to the K model are

$$\begin{aligned} L\frac{dQ}{dt} + RQ + P &= P_p - P_1 + P_2, \\ C\frac{dP}{dt} - Q &= 0, \end{aligned} \tag{11.36}$$

where $L = L_1 + L_2 + L_3$ and $R = R_1 + R_2 + R_3$, P is the pressure jump associated with the capacitance C, P_1 and P_2 are computed by the 3D model, and Q is the flow rate in the circuit.

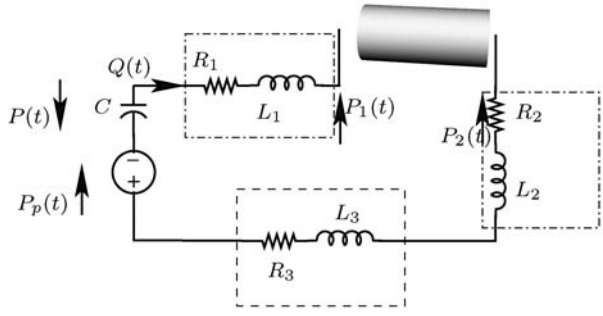

Fig. 11.23. An example of 3D/0D geometrical multiscale model

Assume that both 3D and 0D problems have been properly discretised in time, and the 3D problem also in space, linearised when required. Since the considerations we are going to make are rather general and apply to other couplings like the 3D/1D or the 1D/0D, we indicate with the suffix f the "fine" model (in this case NS) and with c the "coarse" model (here the K model). We also assume that we are using a multistep time advancing scheme for both models, with number of steps $p_f + 1$ and $p_c + 1$, respectively. At each time step we have to solve a linear system in the form

$$\begin{bmatrix} \mathcal{A}_{cc} & \mathcal{A}_{cf} \\ \mathcal{A}_{fc} & \mathcal{A}_{ff} \end{bmatrix} \begin{bmatrix} \mathbf{s}_c^{n+1} \\ \mathbf{s}_f^{n+1} \end{bmatrix} = \begin{bmatrix} \mathbf{b}_c^{n+1} \\ \mathbf{b}_f^{n+1} \end{bmatrix} + \begin{bmatrix} \mathbf{g}_c(\mathbf{s}_c^n, \mathbf{s}_c^{n-1}, \ldots, \mathbf{s}_c^{n-p_c}) \\ \mathbf{g}_f(\mathbf{s}_f^n, \mathbf{s}_f^{n-1}, \ldots, \mathbf{s}_f^{n-p_f}) \end{bmatrix}. \tag{11.37}$$

Vectors $\mathbf{g}_c$ and $\mathbf{g}_f$ account for the terms due to the time advancing schemes in the two submodels, that depend on the solution $\mathbf{s}$ at the previous time steps. Let us denote by N_u and N_p the number of degrees of freedom for velocity and pressure in the fine (NS) model. Suppose moreover to solve the flow boundary problem by means of a Lagrange multiplier approach, so that $\mathbf{s}_f \in \mathbb{R}^{N_u+N_p+1}$ is here given by $\mathbf{s}_f = [\mathbf{U},\ \mathbf{P},\ \lambda]$, while the vector of the unknowns of the coarse model is formed by the state variables of the network, namely $\mathbf{s}_c = [Q,\ P]$. Finally, suppose to use an implicit Euler time discretisation for both the fine and the coarse models ($p_c = p_f = 0$). From (11.36) we have therefore:

$$\mathcal{A}_{cc} = \begin{bmatrix} \frac{1}{\Delta t}L + R & 1 \\ -1 & C \end{bmatrix}, \quad \mathcal{A}_{ff} = \begin{bmatrix} \frac{1}{\Delta t}\mathrm{M} + \mathrm{K} & D^T & \Lambda \\ \mathrm{D} & \mathbf{0} & \mathbf{0} \\ \Lambda^T & \mathbf{0} & \mathbf{0} \end{bmatrix},$$

where M is the mass matrix, K is the discretisation of the diffusion-convection operator of the momentum equation and D is the discretisation of the divergence operator in the NS problem, while the discretisation of the term related to the Lagrange multiplier has been denoted here by Λ.

Once pressure in 3D model is computed for a given flow rate, mean pressures P_1 and P_2 at the interfaces are usually computed by means of quadrature formulae

$$P_k = |\Gamma_k|^{-1} \int_{\Gamma_k} P d\gamma \approx |\Gamma_k|^{-1} \sum_i w_{i,k} p(x_i, y_i, z_i) \qquad k = 1, 2.$$

It is practically convenient to assume that quadrature nodes x_i, y_i, z_i on Γ_k do coincide with nodes of the space discretisation of the problem[7]. We may

[7] In general quadrature nodes will not correspond to grid nodes and interpolation procedures will be necessary.

finally write (see also (11.14)):

$$\mathcal{A}_{cf} = \begin{bmatrix} \mathbf{0}_{1\times N_u} & a_{cf} & 0 \\ \mathbf{0}_{1\times N_u} & \mathbf{0}_{1\times N_p} & 0 \end{bmatrix}, \quad a_{fc,i} = \begin{cases} 0 & \text{if } (x_i, y_i, z_i) \notin \Gamma_{1,2} \\ w_{i,k} & \text{if } (x_i, y_i, z_i) \in \Gamma_{1,2} \end{cases},$$

$$\mathcal{A}_{fc} = \begin{bmatrix} \mathbf{0}_{N_u\times 1} & \mathbf{0}_{N_u\times 1} \\ \mathbf{0}_{N_p\times 1} & \mathbf{0}_{N_p\times 1} \\ -1 & 0 \end{bmatrix},$$

and

$$\mathbf{b}_c^{n+1} = \begin{bmatrix} P_P(t^{n+1}) \\ 0 \end{bmatrix}, \mathbf{b}_f^{n+1} = \begin{bmatrix} \mathbf{F}^{n+1} \\ 0 \\ 0 \end{bmatrix}, \mathbf{g}_c = \begin{bmatrix} \frac{1}{\Delta t} LQ^n \\ 0 \end{bmatrix}, \mathbf{g}_f = \begin{bmatrix} \frac{1}{\Delta t} M\mathbf{U}^n \\ 0 \\ 0 \end{bmatrix}.$$

A possible solution strategy is to solve the complete system (11.37) as a whole at each time step. As already pointed out, also for simple cases as for the example at hand, this approach can have the drawback of a badly conditioned matrix. An alternative approach is a Schur complement decomposition of the problem. By a formal elimination of the coarse solution $\mathbf{s}_c^{n+1}$, we obtain

$$\left(\mathcal{A}_{ff} - \mathcal{A}_{fc}\mathcal{A}_{cc}^{-1}\mathcal{A}_{cf}\right)\mathbf{s}_f^{n+1} = \mathbf{b}_f^{n+1} + \mathbf{g}_2(\mathbf{s}_f^n) - \mathcal{A}_{fc}\mathcal{A}_{cc}^{-1}\left(\mathbf{b}_c^{n+1} + \mathbf{g}_c(\mathbf{s}_c^n)\right). \tag{11.38}$$

In general, matrix $\mathcal{A}_{cc}^{-1}$ is not available and appropriate techniques of solution are required (see the next section). However, in the simplest coarse models like the one at hand, matrix $\mathcal{A}_{cc}^{-1}$ can be easily computed

$$\mathcal{A}_{cc}^{-1} = \frac{1}{(\Delta t^{-1}L + R) + 1}\begin{bmatrix} C & -1 \\ 1 & \Delta t^{-1}L + R \end{bmatrix}, \tag{11.39}$$

and problem can be solved by (11.38). In fact, by a simple algebraic argument, the Schur complement can be explicitly computed

$$\mathcal{A}_{ff} - \mathcal{A}_{fc}\mathcal{A}_{cc}^{-1}\mathcal{A}_{cf} = \begin{bmatrix} \frac{1}{\Delta t}M + K & D & r \\ D^T & \mathbf{0} & \mathbf{0} \\ r^T & -\frac{\Delta t C}{L + \Delta t(R+1)}a_{cf} & \mathbf{0} \end{bmatrix}. \tag{11.40}$$

System (11.38) can be therefore solved, yielding the fine solution $\mathbf{s}_f^{n+1}$. Coarse solution is then recovered by solving

$$\mathbf{s}_c^{n+1} = \mathcal{A}_{cc}^{-1}\left(\mathbf{b}_c^{n+1} + \mathbf{g}_c(\mathbf{s}_c^n) - \mathcal{A}_{cf}\mathbf{s}_f^{n+1}\right).$$

In this way, the coupled problem is split into a sequence of 3D and 0D problems, each of them being in general smaller and better conditioned than the whole heterogeneous system.

11.5.2 Iterative substructuring approaches

The block Gauss elimination procedure proposed in the previous section is seldom feasible, since in general matrix $\mathcal{A}_{cc}^{-1}$ is neither easy nor convenient to compute explicitly. For this reason, here we address some possible solution schemes resorting to the separate computing of the submodels that do not need the explicit computation of $\mathcal{A}_{cc}^{-1}$.

A first, simple method for solving the problem is the following iterative scheme.

1. Let $\mathbf{s}_{f,0}^{n+1}$ be a time extrapolation of $\mathbf{s}_f^{n+1}$ based on the previous time evaluations of $\mathbf{s}_f$.
2. For $k = 0, 1, 2, \ldots$ solve

$$\begin{cases} \mathcal{A}_{cc}\mathbf{s}_{c,k+1}^{n+1} = \mathbf{b}_c^{n+1} + \mathbf{g}_c(\mathbf{s}_c^n, \ldots, \mathbf{s}_c^{n-p_c}) - \mathcal{A}_{cf}\mathbf{s}_{f,k}^{n+1} \\ \mathcal{A}_{ff}\mathbf{s}_{f,k+1}^{n+1} = \mathbf{b}_f^{n+1} + \mathbf{g}_f(\mathbf{s}_f^n, \ldots, \mathbf{s}_c^{n-f_f}) - \mathcal{A}_{fc}\mathbf{s}_{c,k+1}^{n+1} \end{cases} \tag{11.41}$$

   up to the fulfillment of an appropriate convergence test.

Observe how this splitting approach is essentially based on the same fixed point formulation devised for the proof of well posedness of multiscale problems.

The first issue is the *convergence* of the iterations. This problem can be analysed by regarding this scheme as a *block Gauss-Seidel* scheme for solving system (11.37), or, equivalently, as a Richardson preconditioned scheme (see e.g. [403]). By classical arguments, the convergence of the scheme holds if the spectral radius ρ of matrix

$$\begin{bmatrix} \mathcal{A}_{cc} & \mathbf{0} \\ \mathcal{A}_{fc} & \mathcal{A}_{ff} \end{bmatrix}^{-1} \begin{bmatrix} \mathcal{A}_{cc} & \mathcal{A}_{cf} \\ \mathcal{A}_{fc} & \mathcal{A}_{ff} \end{bmatrix},$$

i.e. the maximum modulus of the matrix eigenvalues, is less than 1.

In practice, it is quite hard to compute ρ, so this convergence analysis is seldom able to give quantitative responses about convergence and it has essentially a theoretical relevance. A practical approach for driving the iterative scheme to the convergence is to introduce a parameter to be properly tuned. In the present case, (11.41) can be modified as follows (for the sake of notation we drop time index $n+1$ from now on)

$$\begin{aligned} &\mathcal{A}_{cc}\mathbf{s}_{c,k+1} = \mathbf{b}_c + \mathbf{g}_c(\mathbf{s}_c^n, \ldots, \mathbf{s}_c^{n-p_c}) - \mathcal{A}_{cf}\mathbf{s}_{f,*}^{n+1}, \\ &\mathcal{A}_{ff}\mathbf{s}_{f,k+1} = \mathbf{b}_f + \mathbf{g}_f(\mathbf{s}_f^n, \ldots, \mathbf{s}_f^{n-p_f}) - \mathcal{A}_{fc}\mathbf{s}_{c,k}^{n+1}, \\ &\mathbf{s}_{f,*}^{n+1} = \theta\mathbf{s}_{f,k+1}^{n+1} + (1-\theta)\mathbf{s}_{f,k}^{n+1}. \end{aligned} \tag{11.42}$$

In the example above, this means that average pressures used as forcing terms for the coarse problem are modulated by the *relaxation parameter* θ. An appropriate choice of θ can yield or improve convergence of the iterative scheme, even if a priori it is not easy to identify its optimal value.

This scheme has been used for 3D/1D coupling illustrated in Fig. 11.24. The 3D model features rigid boundaries and mimics a stented segment of a cylindrical artery. Pressure drop problem is solved for the NS model, being pressure computed as a function of the area computed by E model. The latter receives data on flow rate, that are formulated in terms of the incoming characteristic variables (W_2 at interface Γ_{up} and W_1 at interface Γ_{dw}). Velocity and pressure solutions in 3D model (bottom, centre) are illustrated together with area in upstream (bottom, left) and downstream (bottom, right) of Fig. 11.24. Effects of the stent rigidity on the upstream area can be recognised. Relaxation parameter θ has been tuned in this case by a trial and error approach.

The main drawback of this approach is related to the computational costs. Iterations of these coupling algorithm are nested into the time loop, and this in general implies high computational costs. For this reason, more sophisticated algorithms can be devised to reduce the number of iterations. Possible approaches resort to a dynamical choice of relaxation parameters, or to more effective preconditioners of the coupled problem at hand.

Remark 11.5.2 *Splitting schemes like (11.41) or (11.42) can be regarded as the final result of an approximation process starting from a fully accurate model of blood flow problems. If Ω denotes the cardiovascular system (a) in Fig. 11.25, we can summarise the steps performed as follows.*

1. Domain splitting*: Ω is split into Ω_f and Ω_c subdomains ((b) in Fig. 11.25). Original problem is formulated as a set of subproblems. This is the first step of any* domain decomposition method *(see e.g. [408,511]). In domain decomposition theory domain splitting can be performed with or without overlap among subdomains. Here we assume that subdomains do not overlap. Appropriate interface conditions describe the link between two subdomain solutions.*
2. Model coarsening*: Fully model in Ω_c is downscaled to a coarse model ((c) in Fig. 11.25). For lumped parameter models this step requires to keep trace of interface conditions that need to be incorporated in K problem by means of a proper selection of bridging regions.*
3. Iterative substructuring schemes*: Solution of the overall problem is pursued by a sequence of subdomain solutions suitably coupled ((d) in Fig. 11.25). In particular, for coarse K models bridging region compatibility guarantees that in the downscaled problem interface conditions are correctly included.*

This picture based on domain decomposition theory can be useful for the set up and analysis of effective ad hoc preconditioners.

Another approach for reducing computational costs is based on the introduction of a fully explicit splitting of subproblems.

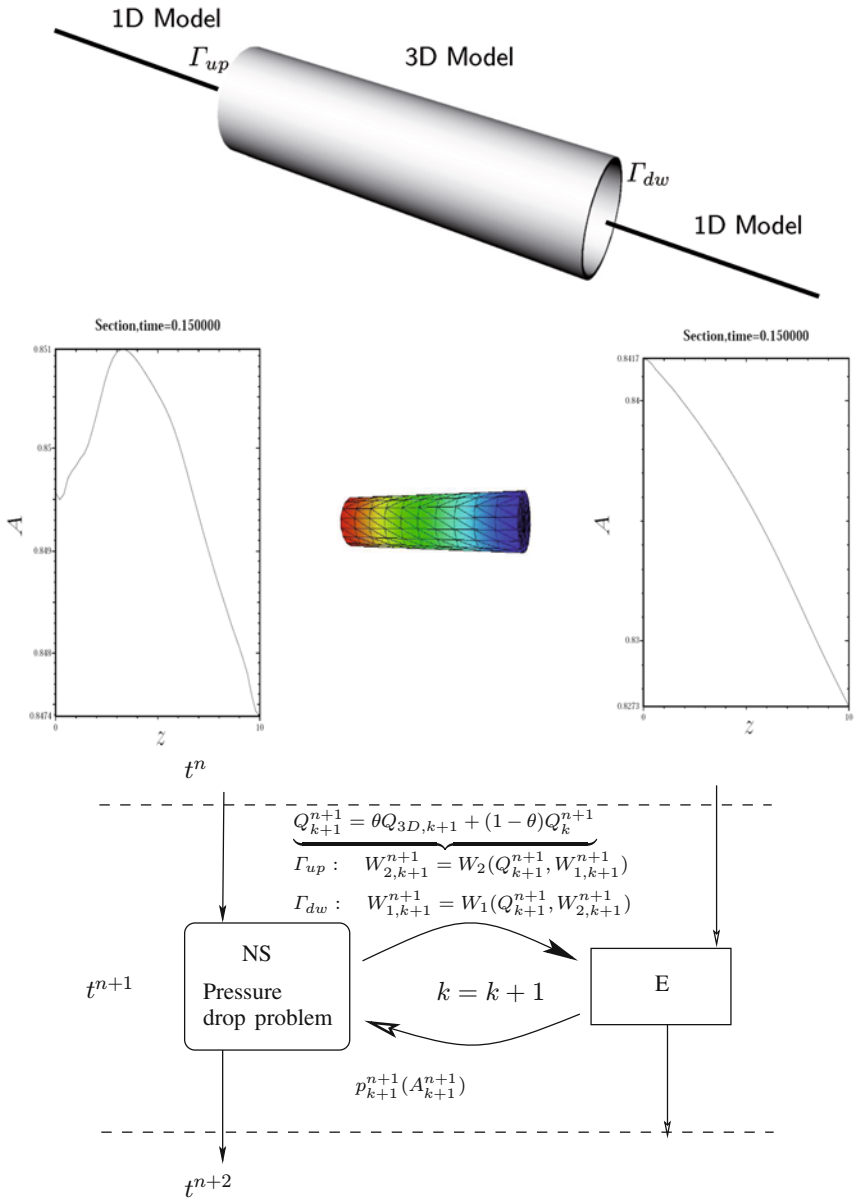

Fig. 11.24. 3D/1D multiscale problem: solution based on an iterative splitting solver with a relaxation parameter θ

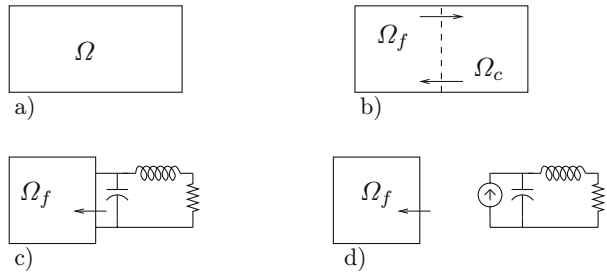

Fig. 11.25. Geometrical multiscale modelling as a domain decomposition method

11.5.3 Decoupled schemes

A simple way for reducing the computational costs essentially relies on the time dependent nature of the problems at hand. At each time step t^{n+1} we compute an extrapolation $\mathbf{s}_f^\star$ of $\mathbf{s}_f^{n+1}$ as a function of the fine solution at the previous time steps and we solve

$$\begin{cases} \mathcal{A}_{cc}\mathbf{s}_c = \mathbf{b}_c + \mathbf{g}_c(\mathbf{s}_c^n, \mathbf{s}_c^{n-1}, \ldots, \mathbf{s}_c^{n-p_c}) - \mathcal{A}_{cf}\mathbf{s}_f^\star \\ \mathcal{A}_{ff}\mathbf{s}_f^{n+1} = \mathbf{b}_f^{n+1} + \mathbf{g}_f(\mathbf{s}_f^n, \mathbf{s}_f^{n-1}, \ldots, \mathbf{s}_f^{n-p_f}) - \mathcal{A}_{fc}\mathbf{s}_c^{n+1}. \end{cases} \tag{11.43}$$

In practise, we perform scheme (11.41) for one time solely. A flow-chart representation of this scheme is given in Fig. 11.26.

The computational advantage is clear, no nested iterations are required. However, both stability and accuracy issues need to be addressed.

1. *Absolute Stability* in time of the scheme is affected by the explicit treatment of the fine solution in the first equation. The region of absolute stability (see Chapter 2) will be reduced even when unconditionally stable time advancing schemes such as implicit Euler are used for the time discretisation.
   A precise quantitative assessment of these stability restrictions is in practise neither easy nor convenient. It is however worth pointing out that in

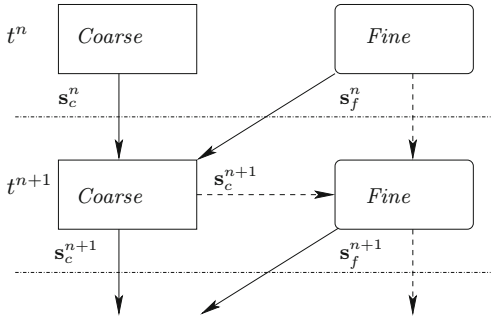

Fig. 11.26. Semi-implicit solver for multiscale problems

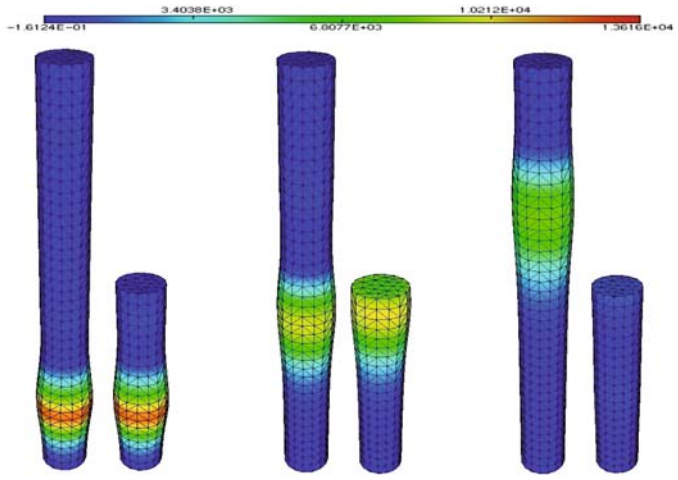

Fig. 11.27. Comparison between the pressure values of the stand-alone and the multiscale solutions at three different times (t=0.005, 0.01 and 0.015), using a 3D linear elastic model for the structure

many situations time advancing schemes used for solving single subproblems are explicit or semi-explicit. This is the case of 3D Navier-Stokes solver with a semi-explicit treatment of the convective term or of Lax-Wendroff schemes for 1D Euler equations (see Chapter 10). Numerical experience suggests that in many situations stability bounds associated with time advancing schemes are not significantly affected by the splitting scheme (11.43). This is the case for instance of results presented in Fig. 11.13.

Another example is provided by the 3D/1D model presented in [159]. In Fig. 11.27 we report a comparison between the pressure computed by a stand-alone 3D compliant model and a multiscale model, solved with a scheme in the form (11.43). Stand-alone model is a 10 cm long tube, the multiscale one is split into two domains (3D and 1D) of 5 cm each. Matching conditions yield the continuity of the total stresses and fluxes. Explicit coupling scheme (11.43) has been successfully used also for the application of multiscale modelling to paediatric surgery, as shown in Section 12.4.

2. *Time Accuracy.* Time accuracy of the scheme (11.43) is not lower than that of the uncoupled scheme (11.41) provided that an appropriate extrapolation $\mathbf{s}_f^\star$ is computed. More precisely, if q_c denotes the accuracy of the time advancing scheme for the coarse problem and q_f the one for the fine problem, an extrapolation of order q_c of $\mathbf{s}_f$ is enough for maintaining an accuracy of order q_c to the solution of the coarse problem. The accuracy of the fine solution will depend both on q_f and q_c. More precisely, on the basis of classical results of numerical analysis (see [268]), it is possible to

prove that accuracy of the fine model is given by:

$$q = \min(q_f, q_c + 1). \tag{11.44}$$

Since it is reasonable that for the fine model one would have a greater accuracy in time than for the coarse model, it follows from (11.44) that, for a desired order of accuracy q for the fine solution, it suffices that the coarse model be solved by a scheme of order $q - 1$.

11.6 Conclusions

Complexity of the vascular system demands for the set up of convenient mathematical and numerical models that go beyond the traditional ones based on Navier-Stokes, Euler or Kirchhoff equations. By themselves, these models have an intrinsic appeal and correctness that make them mathematically and numerically self-consistent. However, when we try to couple them, we face the unusual task of mixing different kind of differential equations, which are not conceived to function in a cooperative model. Many options are possible for yielding a multiscale model, starting from heuristic approaches, that however are often oversimplified and unreliable. From the mathematical and numerical viewpoints, set up of mathematically sound multiscale models raises new challenges both at the theoretical and practical level. The set up of effective and accurate numerical methods for the multiscale modelling and their analysis is not trivial and is actually still an open problem, especially for the simulation of 3D compliant domains. On the other hand, geometrical multiscale approach can play a relevant role in numerical treatment of spurious reflections at the artificial boundaries (see [155]). This approach can be of interest also in other engineering problems, featuring similar geometric multiscale complexity, like the design of intake/out-takes of internal combustion engines, the study of complex hydrological basins for environmental applications, or the design of electrical circuits (see e.g. [6, 116]).

More in general, reliable numerical solution of defective problems is by itself an interesting problem. For instance, in [392] a method for improving the accuracy in blood flow ultrasound measures is proposed, based on the extensive use of numerical simulations with flow rate defective boundary conditions. The focal point of these simulations is the prescription of the flow rate *without* the prescription of a velocity profile that induces a bias in results of ultra sound measurements.

Future perspectives in the mathematics for the vascular system should include *multiscale modelling in time*. Some pathological effects such as plaques formation or aneurysms growth require time scales of weeks, months or even years. Nevertheless, basic mechanisms that could be responsible of these pathologies develop over the time scale of a heart beat (seconds). An adequate multiscale-in-time modelling of these phenomena represents an important challenge for cardiovascular mathematics.